EFFECTS OF ENVIRONMENTAL AGEING PARAMETERS ON INTERFACIAL BOND PROPERTIES OF CARBON FIBER TOW IN EPOXY RESIN-AN EXPERIMENTAL AND NUMERICAL STUDY

by

SHLOKA VEMUGANTI

A THESIS

Submitted in partial fulfillment of the requirements
for the degree of Master of Science
in the Department of Aerospace Engineering
and Mechanics in the Graduate School of
The University of Alabama

TUSCALOOSA, ALABAMA

2009

ABSTRACT

The effects of environment on the interfacial bond strength of carbon fiber tow embedded in epoxy resin are being studied through accelerated aging experiments and pull-out tests (PT). The goal is to examine the synergistic effects of hot, cold, wet, dry and stressed environment on interfacial bond strength (IFBS) of carbon/epoxy composites in order to forecast life of composites in severe environments. The PT specimens were prepared by embedding a fixed length of a carbon fiber tow in uncured epoxy. The interfacial debonding between resin and fiber tow is the targeted mode of failure. A spring loaded frame was designed for applying a preset load to multiple PT specimens. All the PT specimens including the frames with the stressed specimens were subjected to accelerated environmental aging conditions for different time intervals. The moisture absorption and desorption data were recorded. The PT tests were then carried out by pulling the carbon fiber tow from the cylindrical resin, mounted in a screw driven MTS testing machine.

Average IFBS of approximately 21.5 MPa was observed for the unaged control sample. The hot/wet/stressed (70ºC/3% moisture/2 lb) specimens show a significant degradation (-29.03 %) in bond strength after 176 days of aging time. The degradation due to moisture is seen to be more critical under the influence of temperatures (50°C, 70°C). In order to obtain the maximum interfacial shear strength for various embedded lengths and environmental aging parameters, a numerical analysis has been carried out using a 3D finite element model (FEM). A FEM analysis was done using cohesive elements at the fiber/matrix interface in order to study the

environmental aging effects at the interface. The predicted bond strength from the numerical analysis was compared with the experimental data. A reasonable agreement was observed between experimental data and Finite Element Analysis (FEA).

DEDICATION

This thesis is dedicated to everyone who helped me and guided me through the trials and tribulations of creating this manuscript, my mother, my father, my sister, my in-laws and close friends who stood by me throughout the time taken to complete this masterpiece and in particular, my husband who has been very supportive and co-operative.

LIST OF ABBREVIATIONS AND SYMBOLS

FRP	Fiber Reinforced Polymer
IFBS	Interfacial Bond Strength
PT	Pull-Out Test
FEM	Finite Element Model
FEA	Finite Element Analysis
°C	Degree Centigrade
Tg	Glass Transition Temperature of the matrix
CS	Control Sample
CDU	Cold Dry Unstressed
CDS	Cold Dry Stressed
CWU	Cold Wet Unstressed
CWS	Cold Wet Stressed
HDU	Hot Dry Unstressed
HDS	Hot Dry Stressed
HWU	Hot Wet Unstressed
HWS	Hot Wet Stressed
SCET	Stress-Coupled Exposure Tests
CAD	Computer Aided Design
ISS	Interfacial Shear Stress
P	Debond Load

σ	Applied Stress
δ	Displacement
N_3	Nominal Stress - Normal Mode
N_1	Nominal Stress in First Direction
N_2	Nominal Stress in Second Direction
D	Coefficient of Diffusion
M_{inf}	Saturation Moisture Uptake
% M	Percentage Moisture
E_m	Matrix Modulus
E_f	Fiber Modulus
V_m	Matrix Volume Fraction
V_f	Fiber Volume Fraction
τ_{max}	Maximum Interfacial Shear Stress

ACKNOWLEDGMENTS

I would first like to express gratitude to my advisor, Dr. Anwarul Haque and my Co-advisor, Dr. Samit Roy for their guidance and support throughout the research for this thesis. I would like to thank Dr. Mark L. Weaver for serving on my thesis committee. I would like to thank Dr. Piyush K. Dutta, for sub-contracting this project to The University of Alabama and sharing his research expertise. I would also like to thank my colleagues for their constant encouragement. I am grateful to the U.S. Army Construction Engineering Research Laboratory for the financial support offered under contract no. W9132T07C0025 (Phase-II). Finally, I express my deep respect and affection to my parents, my sister and my husband who have always been a source of moral support and inspiration.

CONTENTS

LIST OF TABLES

LIST OF FIGURES

CHAPTER 1

INTRODUCTION

The nature of the adhesion mechanism between the reinforcement and the matrix in a composite material is a complex problem. It has the potential to control the mechanical performance and particularly the durability of the material. Fiber reinforced polymer (FRP) composites provide advantages over conventional structural upgrade systems by offering lower life-cycle costs, often with additional benefits such as easier installation and improved safety. However, no reliable predictive tool is currently available for projecting the future state and durability of composites used in various environments. The failure mechanisms of FRP composites are complex in nature compared to isotropic materials due to presence of multiple constituent materials such as fiber, matrix and interface. In general, fiber fracture, matrix cracking, debonding and delamination are dominant failure mechanisms that are observed in FRP composites. These failure mechanisms are typically governed by the individual properties of the constituent materials. The fiber-resin interface is a key component of fiber-reinforced composites. Among other roles, it provides a means of stress transfer from the matrix to the fibers, and serves to protect the fibers from environmental degradation. The strength of the interfacial bond is thus an important physical property and it is important to investigate the influence of different environmental ageing parameters on the individual constituents of composites, such as fiber, matrix and fiber/matrix interface.

One of the several applied techniques based on specimens with an embedded single fiber filament is the pull-out test. Pulling a fiber out of a matrix button or disk is the simplest way of determining the adhesion strength.

Despite the simple geometry of a single-fiber pull-out test, a closed analytical solution to the stress and strain distributions has not been found and approximate approaches on a shear-lag basis have been shown to provide a coarse qualitative description at best. In this test, one of the most obvious problems is the very inhomogeneous stress state induced in the interface, showing strong gradients at the entry point of the fiber into the matrix drop and at the embedded fiber end. In an ideally elastic model the maximum interface stresses are even infinite and, although in reality the stresses remain limited owing to large strain and plasticity effects, the actual maximum value is very complex and not obtainable by a simple analytical approach. The common data reduction schemes for interpretation of the experimental results rely on very simplistic theoretical ideas, mostly based on the assumption of a constant shear stress distribution along the fiber length, and provide an interface shear strength value. Because of the inadequate theoretical basis, this quantity only represents a mean value of the real interface stress distribution and cannot be expected to be physical measure for interfacial adhesion in the sense of a material property. Numerical analysis is believed to be most promising tool to cope with these challenges and to provide a realistic model of the process.

The current research aims at providing a means for predicting the long-term performance of composite materials, based on accelerated laboratory testing and degradation models.

Laboratory experiments were conducted to study the degradation of IFBS of carbon/epoxy composite using fiber pull-out test due to synergistic influence of moisture, applied stress and temperature. Carbon fiber tow reinforced samples have been used for the pull-out test instead of a single carbon fiber considering the complexity of the tests under the above synergistic environmental ageing conditions. In order to obtain the maximum interfacial shear strength for various embedding lengths and environmental ageing parameters, a numerical analysis has been done using a 3D finite element model. Our aim is to calibrate the model using the experimental results and to predict the degradation in IFBS under different environmental ageing parameters.

CHAPTER 2

LITERATURE REVIEW

Many mechanisms of composites degradation have been reported such as fiber/matrix interfacial debonding, fiber breakage, matrix cracking, delamination, matrix degradation due to chemical exposure, matrix softening, erosion, embrittlement and hydrolysis. The articles that have been reported in the literature describing the mechanisms involved promote one or more modes of degradation listed above. The agents of degradation can be classified under three categories which are environmental, chemical and mechanical. There are sub-categories under each of these categories; these are graphically presented in figure 2.1.

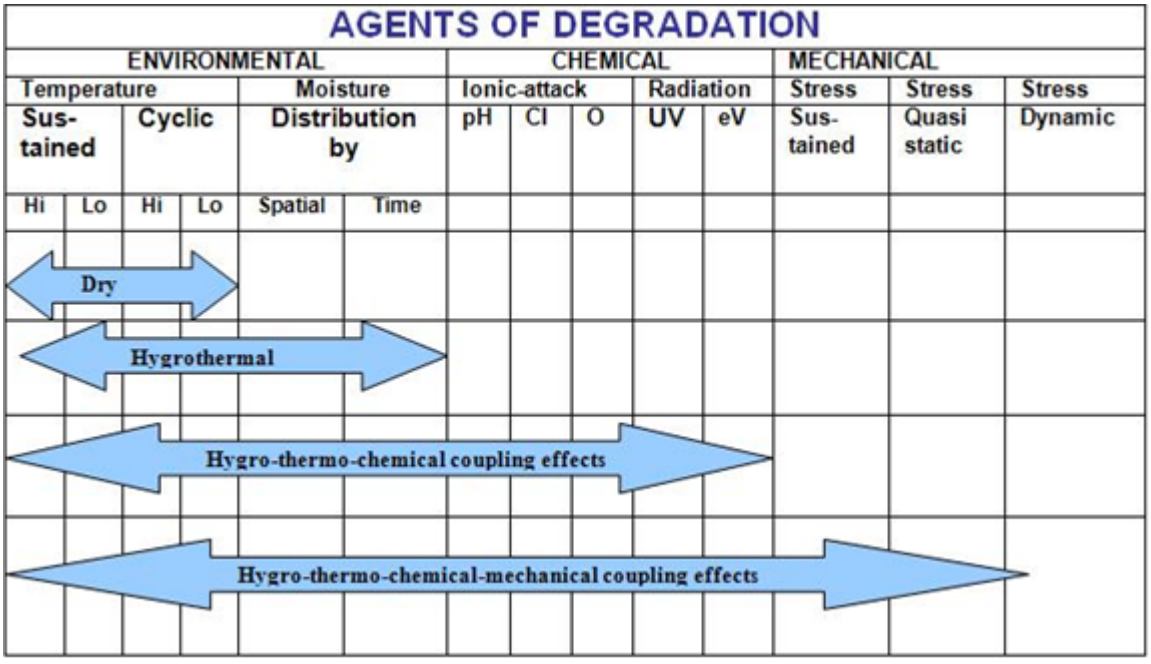

Figure 2.1: Agents of composite degradation

Each degradation agent can work on the composite by itself or in a synergistic combination, moisture alone may cause degradation, but in presence of stress, the magnitude and rate of degradation may both increase nonlinearly. Several studies have been reported on rates of degradation and the mechanisms by each agent or in combination, but, because of the complexities of the processes, there has not been any comprehensive study performed to truly describe the synergistic effect of all the agents when there is a simultaneous interaction on a composite. The agents of all these degradation mechanisms are present in real life and influence the life of the composites, but there is still no model that can suitably predict the process. In the following section we will briefly provide the current state-of-the-art that attempts to describe the processes and predict the degradation rate of the fiber/matrix interfacial bond strength using fiber pull out tests.

2.1 FIBER PULL-OUT TEST

Since the interfacial shear strength is a measure of the integrity of the interface. It is a key property when investigating the micromechanical behavior of composites at the fiber/matrix interface. Accurate evaluation of this parameter has until now been very difficult. In some of the earliest works glass fibers were used which made experiments easier due to their large diameters. Since then many different techniques were reported for evaluating the bond strength out of which single fiber pull-out test came close to the satisfactory test method requirements. As for the other methods involving the tedious and hazardous handling of single fibers, the technique may be disappointing, in proportion to the rate of success that is currently achieved at the end of the tests

and that may be as poor as 25% according to Piggott & Andison [1987]. Nevertheless, the method has been extensively applied since many years to a large number of fibers and matrices: glass [Shiriajeva & Andreevskaya, 1962; Andreevskaya & Gorbatkina, 1972; Emadipour & al, 1982; Chua & Piggott,1985], carbon [Favre & Perrin, 1972; Penn & al., 1985; Piggott & al., 1986], aramid fibers [Eagles & al., 1976; Favre & Merienne, 1981; Penn & al., 1982, 1983, 1984, 1985], high-modulus polyethylene [Ward & Ladizesky, 1985; Nardin & Ward,1987], basalt [Subramanian & Shu, 1985], etc…For large diameters fibers or bundles of thin filaments as in carbon-carbon materials, pull-out may be obtained by pushing the "fiber" out of a very thin slice of the "matrix". Similarly, pull-out can be applied to bundles of fibers [Mai & Castino, 1985]. There are in fact also good reasons to think that bundles retain some characteristics as a whole in the molded composites and that the bundle-matrix interface may be of interest [Wells & Beaumont, 1985].

2.2 ENVIRONMENTAL AGEING

Moisture absorption characteristics and degraded mechanical properties comprise an important part of durability studies of composites. Since the water has to be transferred from the matrix to the fibers, and further again to the matrix, it is expected that the nature of the fiber-matrix interface might play a role in the hygrothermal behavior of carbon epoxy composites. Damage due to applied stress and/or moisture diffusion and temperature also plays a major role in composite absorption behavior. Some studies have reported increased diffusion but unchanged concentration while others reported unchanged diffusion but increased moisture concentration.

The potential effects of temperature are similar to that of moisture. Carbon fibers tend to be unaffected up to temperatures of 600 °C in inert atmosphere. It is well recognized that the mechanical behavior of many composite materials depends largely on the properties of the fiber/matrix interface. Though some research has been done on the individual/coupled influence of moisture, stress and temperature on carbon/epoxy composites; there has been no comprehensive attempt to predict the interfacial bond strength degradation due to the synergistic influence of the above parameters.

Single fiber pull-out tests were successfully carried out to investigate the influence of water absorption on the fiber/matrix interfacial properties of aramid/epoxy composite (Kazuto Tanaka, Kohji Minoshima, Witold Grela and Kenjiro Komai). They had observed that the interfacial strength of aramid/epoxy composite was decreased by 26% after 7 week immersion time in deionized water at 80 °C.

Pull-out tests were performed in order to measure the interfacial strength between the rebar and a concrete matrix (Abdolkarim Abbasi, Paul J. Hogg). Glass fiber reinforced plastic rods investigated in their work were subjected to alkaline solutions at 60 °C for three different exposure times, i.e. 30, 120 and 240 days. Their results show that the tests at lower temperatures, i.e. 20, 40 and 60 °C increased the bond strength by more than 40% after 8 months immersion compared to 1 month immersion. At higher temperatures, i.e. 80, 100 and 120 °C, the bond strengths for samples immersed for 240 days were 10–30% greater than for those samples

immersed for 1 month. They concluded that reduction in interfacial bond strength for all samples tested appeared to depend primarily on the temperature of the pull-out test.

2.3. NUMERICAL ANALYSIS

Studying single-fiber pull-out problems has been emphasized for understanding fiber/matrix interface mechanism and for determination of the stress distribution and strength along and within the constituents as well as their interfaces. Solutions sought to investigate the fiber pull-out problems were based on the following three approaches: analytical method, numerical approach, and experimental test.

Numerical analyses for single fiber pull-out at different bonded interfaces were reported for a perfectly bonded interface (Grande et al.) and for a frictionally bonded interface (Faber et al.). Further finite element analyses were also reported for mechanics of the pull-out at different interface conditions (Pochiraju) and for the assessment of interfacial stress transfer mechanisms, shear stress distribution along the fiber inside the resin, and effect of the graded interphase properties (Nishiyabu et al.).

The CAD-based heterogeneous fiber and matrix assembly was developed to model the composite single-fiber pull-out problem. The integrated CAD/FEA was conducted to simulate the fiber pull-out mechanism assuming perfect bonding between fiber and matrix at the interface. (Sun, W. and Lin, F). The effect of the number of modeling elements, matrix/fiber stiffness ratio,

and embedded fiber cross sections on the axial stress and interface shear stress in the fiber and matrix were also analyzed.

CHAPTER 3

EXPERIMENTAL WORK

3.1. MATERIALS

The fiber pull-out samples consisting of a carbon fiber tow embedded in epoxy resin were used in this study. A single carbon fiber tow has been used instead of single carbon filament for simplicity of the test. The polymer matrix was SC-780, a two component toughened epoxy resin supplied by Applied Poleramic Inc, USA. Part-A consists of 60-70% diglycidylether of bisphenol A, 10-20% aliphatic diglycidylether and 10-20% epoxy toughener. Part-B is a hardener consisting of 70-90% aliphatic amine and 10-20% triethylenetetramine. The mixing ratio of resin to hardener was 100 to 22 by weight. The carbon fiber used was HMF CU160, supplied by SciArt Inc., Canada. A spool of Carbon fiber tow having 6000 filaments in each tow was used. Cross section of the carbon fiber tow was $34x10^{-5}$ in^2.

3.2. SPECIMEN PREPARATION

3.2.1. Apparatus

The required items needed to prepare the carbon fiber pull-out specimens are hand gloves, nose mask, hollow cylindrical mould with grooves, a base plate, holding window frame, FREEKOTE, release film, release fabric, spring clamps, carbon fiber tow, SC-780 epoxy resin, hardener, measuring scale, silver marker, stirrer, gluing tape and wipes.

3.2.2. Specimen Mould Design

Manufacturing of the fiber pull-out specimens required a special mould design consisting of a hollow cylindrical mould with groves, a base plate and a holding window frame assembly as shown in figure 3.1. The mould was manufactured in UA mechanical workshop.

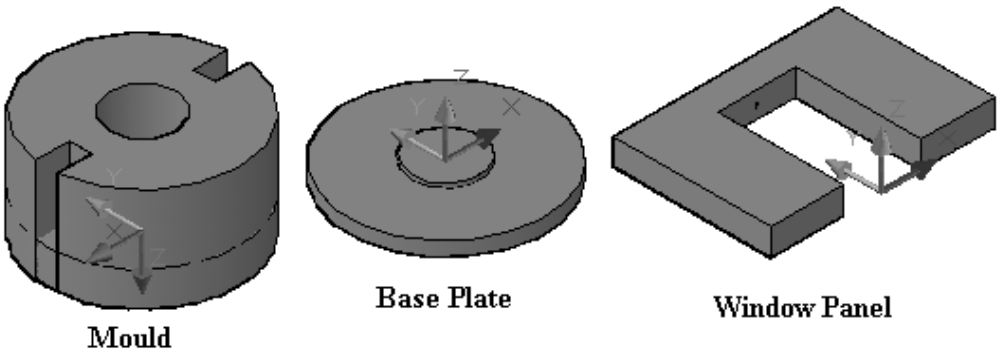

Figure 3.1: Fiber pull-out specimen mould design

3.2.3. Procedure for Specimen Preparation

Four pieces of release film and one piece of release fabric each of diameters greater than the base plate were cut. The release fabric was placed in between the release films like a sandwich. The sandwich of release film and fabric were placed on the base plate. The bottom of the hollow cylinder was closed with base plate ensemble. These measures were taken in order to prevent the resin from leaking. To keep the base plate fixed in position two spring clamps were placed one on each end as shown in Figure 3.2. Release FREEKOTE was sprayed inside the mould. This helped in removing the sample from the mould with ease after it hardened. The excess free coat was wiped off the mould and was left to dry. A known length of carbon fiber

tow was cut from the spool and a 2 mm marking measured from the tow end was made on it with a silver marker. Resin and hardener were mixed in the ratio 4:1 by volume. The mixture was then carefully poured into the mould up to the brim. It was made sure there was no leakage of the resin near the separation of the base plate and the cylinder. The fiber was then placed on the window frame with the help of gluing tape. The window frame was then inserted through the grooves provided in the mould, embedding the fiber tow into the resin up to the marking line ensuring the alignment of the fiber. The whole setup was left undisturbed at room temperature for 24 hours after which the sample was pushed out of the mould and was left for post curing at 71°C for 6 hours in the oven. Figure 3.2 shows a manufactured fiber tow pull-out specimen.

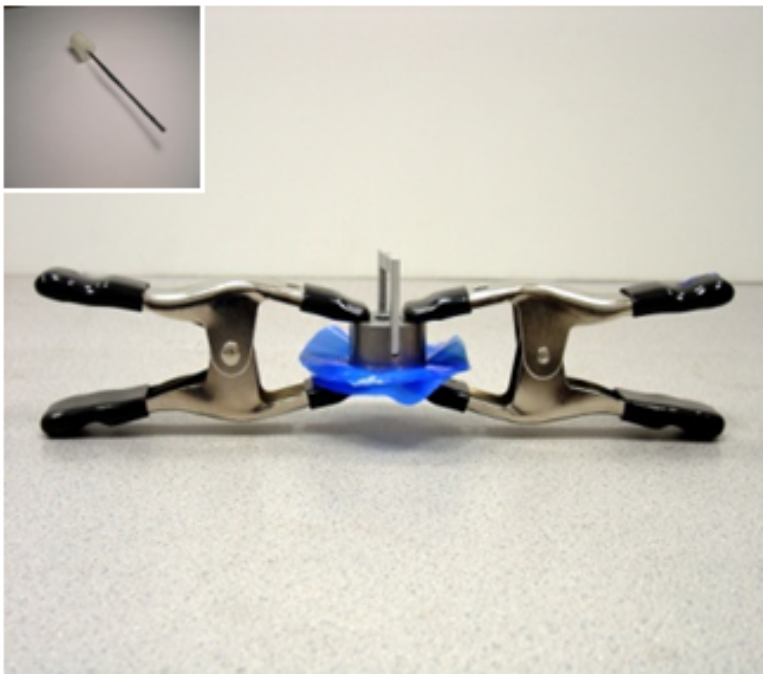

Figure 3.2: Experimental set-up for manufacturing the fiber pull-out specimens and a manufactured fiber pull-out specimen

3.2.4. Post Manufacturing

The specimens were immersed in a dessicator with silica crystals until the moisture desorption process took place.

3.2.5. Safety Measures

- Care must be taken while mixing the resin and hardener as the matrix starts to gel if the mixing is done for a longer time.
- Wearing hand gloves at all times during the specimen preparation is necessary as the carbon fiber could penetrate into the skin.
- Wearing a nose mask is necessary when preparing the specimen as it is not advisable to inhale the chemicals and the fibers.

3.3. ENVIRONMENTAL AGEING

3.3.1. Accelerated Environmental Ageing Conditions

Two temperature conditions were selected for accelerated ageing.

- HOT, operating at 70 °C
- COLD, operating at 50 °C

The choice of these temperatures was made making the **Arrhenius rate law** as the basis, this states that the rate of a chemical reaction increases exponentially with the absolute temperature. It also states that for many reactions which occur near room temperature, a

temperature increase of 10 ^{o}C approximately doubles the rate of the reaction**.** And also in order to keep the aging temperature away from the Tg of the materials (~93.33 ^{o}C).

Depending on the exposure test requirements the specimens were subjected to nine different environmental ageing conditions. Each of those is tabulated in Table 3.1.

Table 3.1: Sample designation as per exposure test conditions

Environmental Exposure Condition	Aging time t=0	Aging time t= t_1 hrs.	Aging time t= t_2 hrs.	Total
Unaged (Control)	4 CS00-0	-	-	4
Cold/dry/unstressed	-	4 CDU-1	4 CDU-2	8
Cold/dry/stressed	-	4 CDS-1	4 CDS-2	8
Cold/wet/unstressed	-	4 CWU-1	4 CWU-2	8
Cold/wet/stressed	-	4 CWS-1	4 CWS-2	8
Hot/dry/unstressed	-	4 HDU-1	4 HDU-2	8
Hot/dry/stressed	-	4 HDS-1	4 HDS-2	8
Hot/wet/unstressed	-	4 HWU-1	4 HWU-2	8
Hot/wet/stressed	-	4 HWS-1	4 HWS-2	8
Total Specimens	4	32	32	68

In Table 3.1: H (hot (70°C)), C (cold (50°C)), W (wet (immersed in de-ionized water)), D (dry), S (stressed), U (unstressed). 1, 2 at the end of each sample group designation represent the first and second time intervals when the sample group was pulled out for fiber pull-out test. For

example, sample group CDU1 represents the sample group, which was exposed at 50 °C in a dry environment, but was not stressed and was withdrawn at the first interval of time.

3.3.2. Stress-Coupled Exposure Tests

A unique test configuration was developed for stress-coupled exposure tests (SCET) of fiber pull-out specimens as shown in Figure 3.3. A number of tension springs were used to apply tension on the fiber tow pull out specimens; which were mounted on a steel frame. The tension was adjusted by providing calibrated displacement of the spring as per the spring constant. A load of 2 lb was applied on each sample. The spring constant of the springs used was 15.58 lb/in. For the respective load and spring constant the displacement of the spring was 0.25673 in.

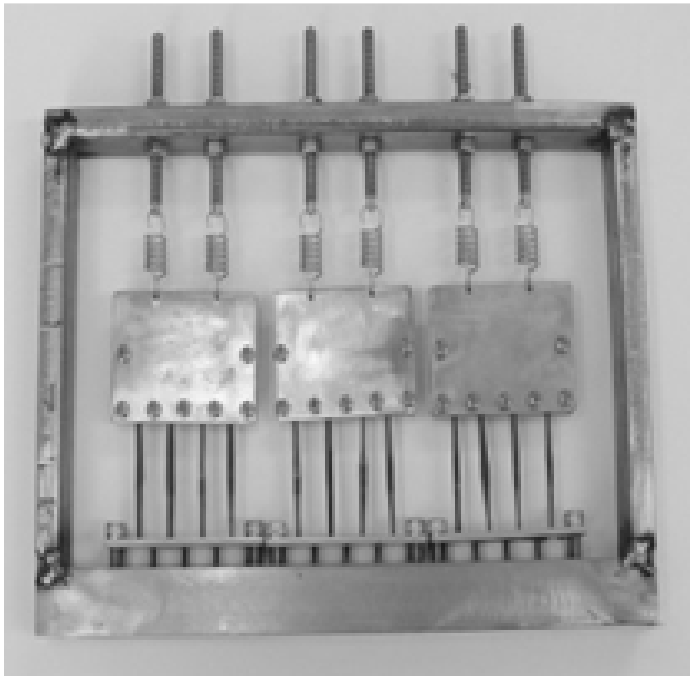

Figure 3.3: Stress Coupled exposure test fixture

3.3.3. Explanation of the Environmental Ageing Conditions

- Unaged (Control): All the samples designated as CS00 have been subjected to physical ageing at room temperature. These were kept in a dessicator until these were tested.
- Cold/dry/unstressed: All the samples designated as CDU were unstressed and exposed to dry atmosphere at 50 °C.
- Cold/dry/stressed: All the samples designated as CDS were stressed and exposed to dry atmosphere at 50 °C.
- Cold/wet/unstressed: All the samples designated as CWU were unstressed and were immersed in a water bath at 50 °C in an environmental chamber.
- Cold/wet/stressed: All the samples designated as CWS were stressed and were immersed in a water bath at 50 °C in an environmental chamber.
- Hot/dry/unstressed: All the samples designated as HDU were unstressed and exposed to dry atmosphere at 70 °C.
- Hot/dry/stressed: All the samples designated as HDS were stressed and exposed to dry atmosphere at 70 °C.
- Hot/wet/unstressed: All the samples designated as HWU were unstressed and were immersed in a water bath at 70 °C in an environmental chamber as shown in figure 3.4.
- Hot/wet/stressed: All the samples designated as HWS were stressed and were immersed in a water bath at 70 °C in an environmental chamber as shown in figure 3.4.

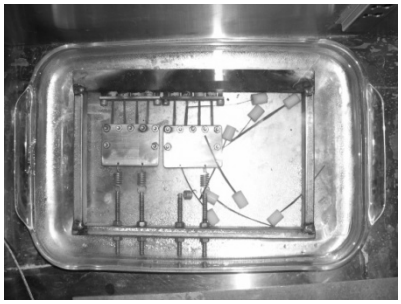

Figure 3.4: Unstressed and Stressed samples immersed in water at 70°C, HWU and HWS ageing conditions

3.4. FIBER PULL-OUT TEST

Pull out tests were performed to determine the interfacial bond strength (IFBS) of the carbon/Epoxy composites. IFBS is mostly matrix dominated and various environmental degradation mechanisms such as moisture and temperature are more active in the matrix materials. Carbon fiber tow pull out specimens were considered in pull out test to produce interfacial bond failure between matrix and fiber. The setup for fiber pull out test is shown in Figure 3.5.

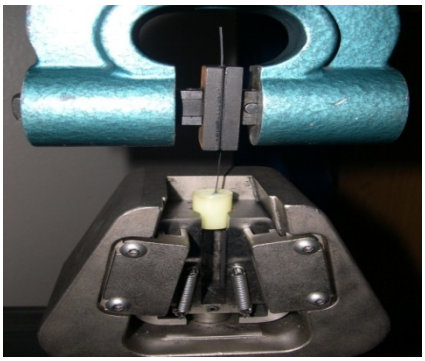

Figure 3.5: Experimental test setup

The tests were performed using a 5,000 lbs load capacity MTS testing machine. The rate of the crosshead motion was maintained at 0.02 in/min. The load was applied to the specimen and the load-displacement data were plotted for each ageing condition. At least four test specimens were considered for each aged condition.

CHAPTER 4

FINITE ELEMENT MODEL DEVELOPMENT

4.1. FINITE ELEMENT METHOD

Finite element method also referred to as Finite element analysis (FEA) is a fairly recent discipline crossing the boundaries of mathematics, physics, engineering and computer science. The method has wide application and enjoys extensive utilization in the structural, thermal and fluid analysis areas. The finite element method is comprised of three major phases:

- Model Development: The analyst develops a finite element mesh to divide the subject geometry into sub domains for mathematical analysis, and applies material properties and boundary conditions, and applied load.
- Solution: The program derives the governing matrix equations from the model and solves for the primary quantities.
- Post-Processing: The analyst checks the validity of the solution, examines the values of primary quantities (such as displacements and stresses), and derives and examines additional quantities (such as specialized stresses and error indicators).

The advantages of FEA are numerous and important. A new design concept may be modeled to determine its real world behavior under various load environments, and may therefore be refined prior to the creation of drawings, when few dollars have been committed and changes are inexpensive. Once a detailed CAD model has been developed, FEA can analyze the

design in detail, saving time and money by reducing the number of prototypes required. An existing product which is experiencing a field problem, or is simply being improved, can be analyzed to speed an engineering change and reduce its cost. In addition, FEA can be performed on increasingly affordable computer workstations and personal computers, and professional assistance is available.

4.2. ROLE OF FEA IN THIS PROJECT

Finite element analysis is a well known platform and has proved to provide good results for solid mechanics problems. Having selected ABAQUS, Standard finite element commercial software package the analysis was done on the fiber pull-out model to give the maximum interfacial bond strength.

The major focus in this research is to analyze fiber pull-out test specimens under various environmental ageing conditions using finite element model in order to predict synergistic ageing effects on interfacial bond strength. The predicted FEA results are intended to calibrate through experimentally determined interfacial bond strength. Eventually the predicted bond strength will be incorporated in a computer code to be developed for the life prediction of composite materials in harsh environments.

4.2.1. Major Goals

The following major goals are set in the finite element analysis of this research:

- To develop geometric model of fiber pull-out test specimens and simulate applied stress (σ) vs. displacement (δ) plots for defined ageing conditions.
- To calibrate the predicted σ-δ plot to match with the experimental σ-δ plot.
- To establish degraded material properties under synergistic environmental aged condition for life prediction of composite materials.
- To simulate interfacial debonding in FEA model using cohesive element to establish appropriate failure model.

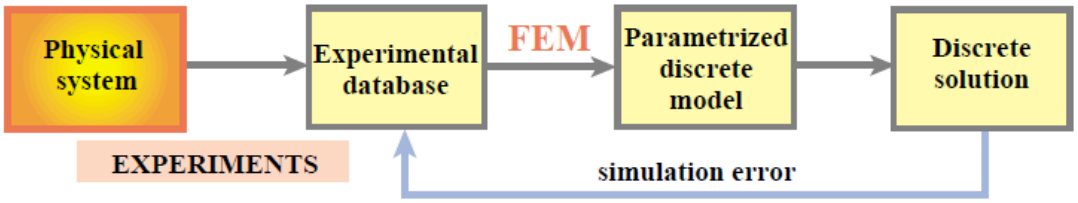

Figure 4.1: Flow chart depicting the FEM analysis

4.2.2. Approach

Figure 4.1 shows a schematic flow chart of the proposed research task under finite element analysis. Considering a physical system, experiments are performed. The results from the experiments such as pull-out load are fed into the FEA model with appropriate boundary conditions. Analysis would then be done to achieve a discrete solution. The results from FEM analysis and Experiments would be matched and checked for calibration parameters.

In experiments the specimens were subjected to various synergistic environmental ageing effects, due to which the specimens degraded. The idea was to incorporate the experimental data

like moisture uptake, temperatures etc, into the fiber/matrix interface in the finite element model in order to obtain realistic results that would match the experimental results. The fiber/matrix interface is shown in figure 4.2.

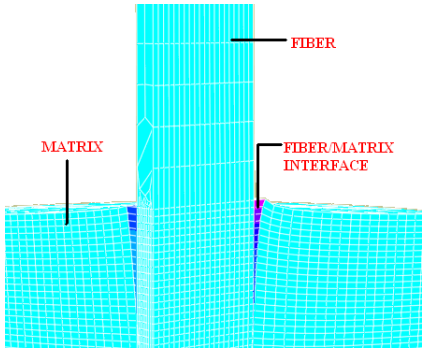

Figure 4.2: Fiber/Matrix Interface in the FEA model

4.3. FINITE ELEMENT MODEL FOR FIBER TOW PULL-OUT TEST WITHOUT COHESIVE ELEMENTS (3D, QUARTER SYMMETRY MODEL)

Considering an unaged (Control-CS00) specimen, a three dimensional fiber tow pull-out quarter symmetry model was developed using ABAQUS FEA code. The steps required to develop the FEA model for analysis are as follows:

- Model the 3D quarter symmetric geometry.
- Assign the sections to the fiber and matrix.
- Incorporate the fiber and matrix properties.
- Define the loading conditions and the Boundary conditions as per the requirement.
- Generate the mesh.
- Carryout the analysis.

4.3.1. Material Properties

The properties of the fiber and the matrix are given in Table 4.1. The elastic constants of the unidirectional composite were predicted using rule of mixtures. The stiffness matrix for the transversely anisotropic composite was determined and the values are provided in table 4.2.

Table 4.1: Material properties of HMF CU160 Carbon fiber and SC-780 Epoxy resin

Tensile Modulus (E_f)	255000 MPa
Poisson's Ratio (ν_f)	0.33
Modulus (E_m)	2826.85 MPa
Poisson's Ratio (ν_m)	0.39

Table 4.2: Orthotropic Stiffness properties in the fiber in FEA model

Stiffness Components	(MPa)
D1111	13113
D1122	7404
D2222	13113
D1133	8480
D2233	8480
D3333	22753
D1212	19158
D1313	22753
D2323	2855

4.3.2. Loading and Boundary Conditions

A uniform pressure load was applied in FEA on the fiber end as shown in figure 4.3. A maximum failure load of 323.20 N (P) was observed in unaged control specimen in the pull-out test. The model being quarter symmetric the debond load (P) was divided by four and the resultant load of 80.80 N (P/4) was applied in the model.

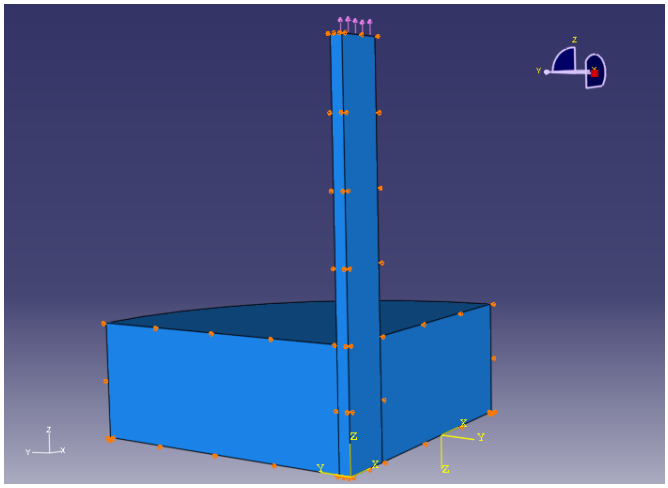

Figure 4.3: Loading and Boundary Conditions on the fiber tow pull-out model

Boundary Conditions were applied similar to the conditions prevalent during the experimental testing. As seen in figure 4.3 roller supports were used for movement along the fiber direction (U3). In the X- direction U2 (Y-axis) was fixed and in the Y-direction U1 (X-axis) was fixed. The outer rim and the base of the matrix were fixed completely.

4.3.3. Mesh Generation

The analysis results were mostly dependent on refinement of the mesh. The result is improved with finer mesh and Linear quadratic, 8 noded brick elements were used to generate the mesh on the pull-out model as shown in figure 4.4.

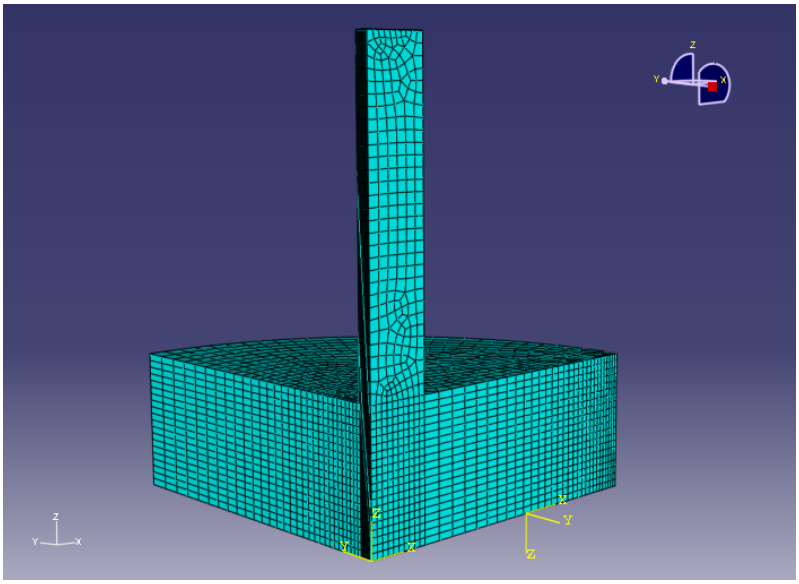

Figure 4.4: Mesh generated on the fiber tow pull-out model

4.4. FINITE ELEMENT MODEL WITH COHESIVE ELEMENTS IN THE FIBER/MATRIX INTERFACE

In order to observe separation of the fiber from the matrix in the FEA model and to incorporate the environmental ageing effects, cohesive elements were inserted at the fiber/matrix interface as shown in the figure 4.5. The analysis was done using traction separation law. Initially, the model was made to work without cohesive elements for the unaged control specimen assuming perfect bonding at the fiber/matrix interface. Most degradation in interfacial bond strength was expected at the fiber/matrix interface, hence the degradation study was concentrated in that region.

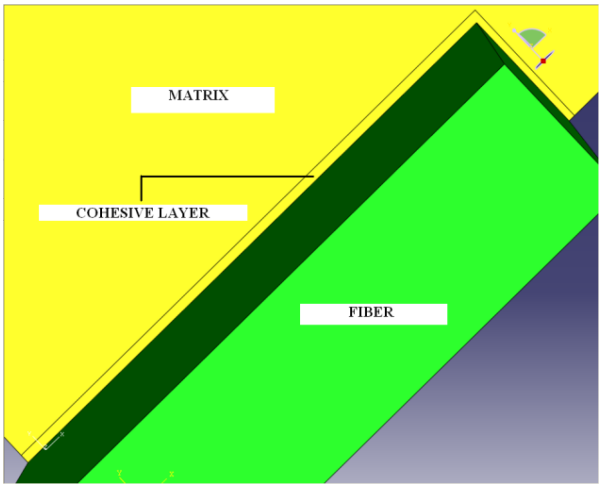

Figure 4.5: Cohesive elements in the fiber/matrix interface

Similar to the model developed without cohesive elements at the interface, this model with cohesive elements was modeled considering an unaged (Control-CS00) specimen, and a three dimensional fiber tow pull-out quarter symmetry model was developed in ABAQUS, Standard. The steps required to develop the FEA model for analysis with cohesive elements are as follows:

- Model the 3D quarter symmetric geometry of the fiber, matrix and cohesive layer as separate parts and then assembling them together. This was done to avoid mesh distortion problems near the cohesive layer.
- Assign the sections to the fiber, matrix and cohesive layer. When assigning a section to the cohesive layer choose the option as cohesive.
- Incorporate the fiber, matrix and cohesive layer properties.
- Define the loading conditions and the Boundary conditions as per the requirement.

- Generate the mesh.
- Perform the analysis.

4.4.1. Material Properties

Same material properties were used for fiber and matrix that were used in the model without cohesive elements. To define cohesive layer material properties Maxs Damage was chosen from the drop down menu in Damage for Traction Separation Laws (ABAQUS), which was under the Mechanical category as shown in the figure 4.6.

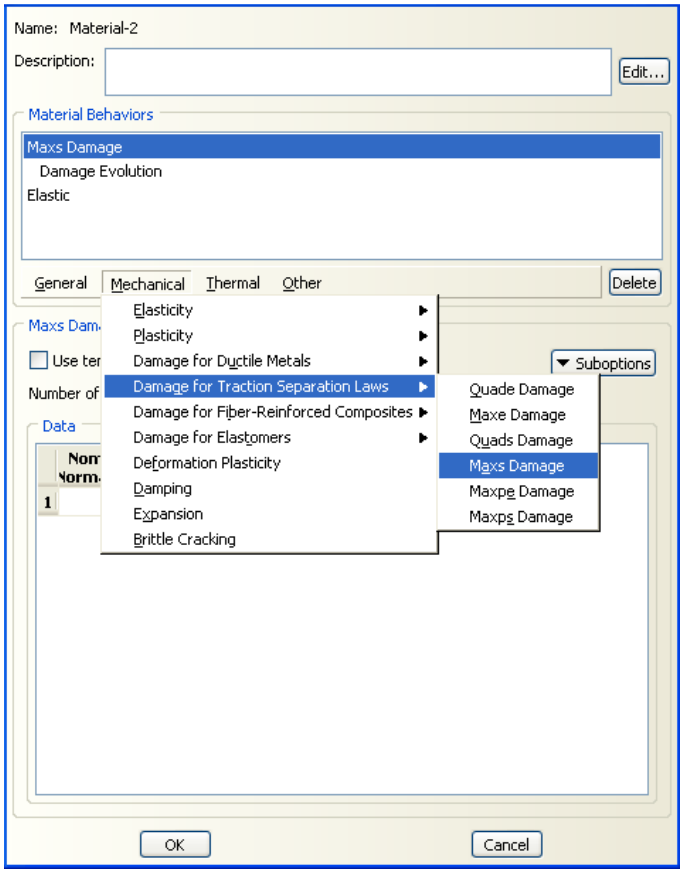

Figure 4.6: Cohesive layer material properties

When the window for Maxs Damage opens it asks for Nominal Stress - Normal Mode (N_3), Nominal Stress in First Direction (N_1) and Nominal Stress in Second Direction (N_2). These values vary with each ageing condition which would be discussed in the next chapter. In the sub options in the Maxs Damage window is Damage Evolution, this value was kept constant for all cases which was 0.25. All the default properties were kept in the Damage Evolution window, the Mode Mix Ratio was chosen as Traction. Elastic was chosen from the drop down menu in Elasticity, which was under the Mechanical category which is seen in figure 4.6. Here in this window the type was selected as traction and the Moduli time scale (for viscoelasticity) was chosen as Instantaneous and the stiffness values E, G1 and G2 were entered which vary for different ageing conditions which would be discussed in the next chapter.

4.4.2. Loading and Boundary Conditions

Loading condition was similar to the model without cohesive elements. The experimental load (P) was divided by four and the resultant load was applied (P/4). The loads were different for each ageing condition.

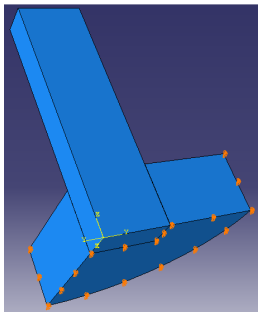

Figure 4.7: Loading and Boundary Conditions on the fiber tow pull-out model with Cohesive Elements

Boundary Conditions were applied similar to the conditions prevalent during the experimental testing. As seen in figure 4.7 the outer rim and the base of the matrix were fixed completely.

4.4.3. Mesh Generation

ABAQUS geometric model development code was used in mesh generation. An independent instance was defined on the assembly before generating the mesh and an 8-node linear brick, reduced integration, hourglass control were chosen from ABAQUS code to generate the mesh on the fiber and matrix. An 8-node three-dimensional cohesive element was used to generate the mesh on the cohesive layer. Mesh Tie constraint was used to tie the mesh in the cohesive layer region. This was done to reduce run time and mesh distortion problems. Figure 4.8 shows the mesh on the model with cohesive elements.

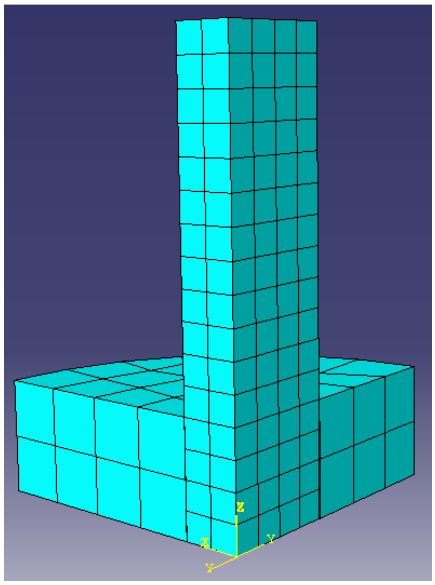

Figure 4.8: Mesh generated on the fiber tow pull-out model with Cohesive Elements

CHAPTER 5

RESULTS AND DISCUSSION

5.1. MOISTURE ABSORPTION AND DESORPTION

In order to lose moisture (desorption) after manufacturing, the fiber tow pull-out specimens were left in the dessicator with silica crystals. These specimens were then subjected to the previously mentioned environmental ageing conditions such as hot/wet/unstressed, cold/wet/stressed etc; in the wet conditions the specimens absorbed certain amount of moisture. These readings were recorded and are presented in this chapter.

5.1.1. Moisture desorption data

Figure 5.1 shows moisture loss (desorption) vs square root of time (sqrt time (t)) plots of the fiber tow pull-out specimens.

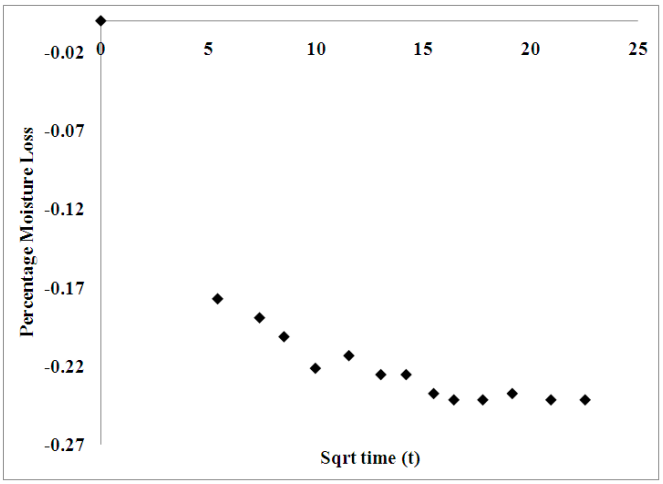

Figure 5.1: Moisture desorption vs Sqrt time (t) plot

The nature of the desorption plot in Figure 5.1 shows steeper slope in early stage indicating increased moisture loss (0.18%) in the first 25 hours and then in four weeks moisture loss reaches to a maximum of 0.23 % maintaining almost constant weight of the sample. It is to be noted that post curing temperature of the resin was 70^0C and the same temperature was maintained in the dessicator for the controlled sample in order to avoid post curing effects at later ageing experiments. Such trend of post curing at elevated temperature experiment was reported in earlier work.

5.1.2. Moisture absorption data

The WET specimens were weighed periodically to observe the moisture gain in them. Figure 5.2 shows moisture uptake (absorption) vs square root of time (sqrt time (t)) plots of the hot/wet/unstressed (HWU) and hot/wet/stressed (HWS) fiber tow pull-out specimens.

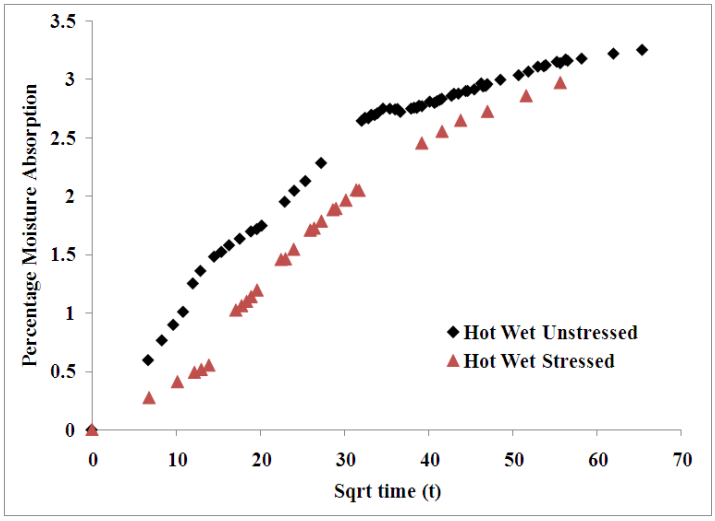

Figure 5.2: Moisture absorption vs Sqrt time (t) for HWU and HWS

The HWU specimens absorbed moisture more rapidly than the HWS specimens reaching a maximum of 3.25% in 4274 h (178 days) exposure time. The HWS specimens absorbed lesser percentage of moisture than the HWU specimens attaining a maximum of 2.97% in an exposure time of 3096 h (129 days). The possible reason could be the lesser exposure time than the HWU specimens.

Figure 5.3 shows moisture uptake (absorption) vs square root of time (sqrt time (t)) plots of the cold/wet/unstressed and cold/wet/stressed fiber tow pull-out specimens.

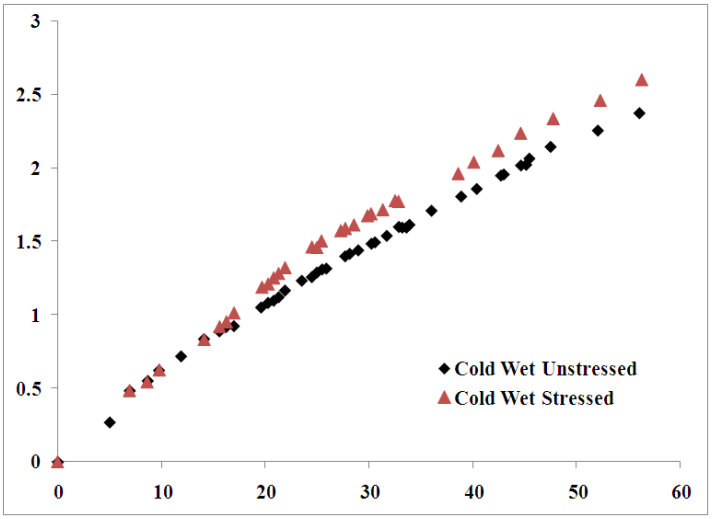

Figure 5.3: Moisture absorption vs Sqrt time (t) for CWU and CWS

The moisture absorption was observed to be similar for both CWU and CWS cases in the initial stages, but at a later time CWS absorbed moisture more rapidly than CWU, reaching a maximum of 2.60% in an exposure time of 3167 h (132 days). The reason could be the opening

up of cracks in the stressed specimens leading to more moisture intake. The CWU specimens absorbed a maximum of 2.37% moisture in 3145 h (131 days) exposure time.

Coefficient of Diffusion (D) and saturation moisture uptake (M_{inf}) for each WET ageing condition, based on experimental data, were calculated using a method developed by (Roy, Vengadassalam and Wang). A MATLAB code was developed to evaluate coefficient of diffusion and saturation moisture uptake (Appendix A). After calculating the coefficient of diffusion and saturation mass uptake, this data was used in another code (Appendix B) to plot ficks law along with experimental data for each ageing condition as show in figures 5.4 through 5.7.

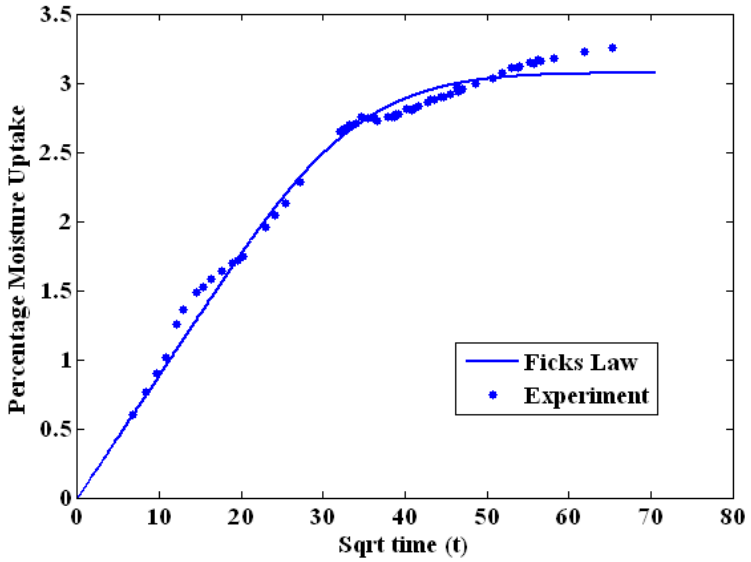

Figure 5.4: Percentage moisture uptake vs Sqrt time (t) for HWU specimens

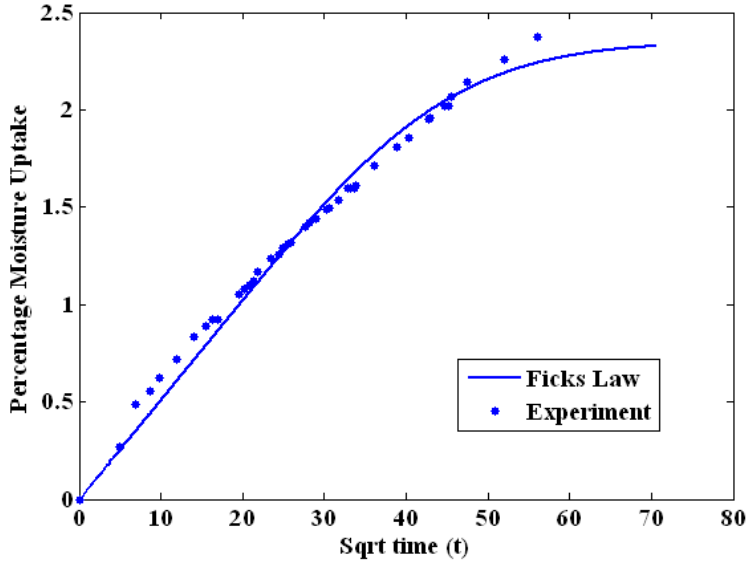

Figure 5.5: Percentage moisture uptake vs Sqrt time (t) for CWU specimens

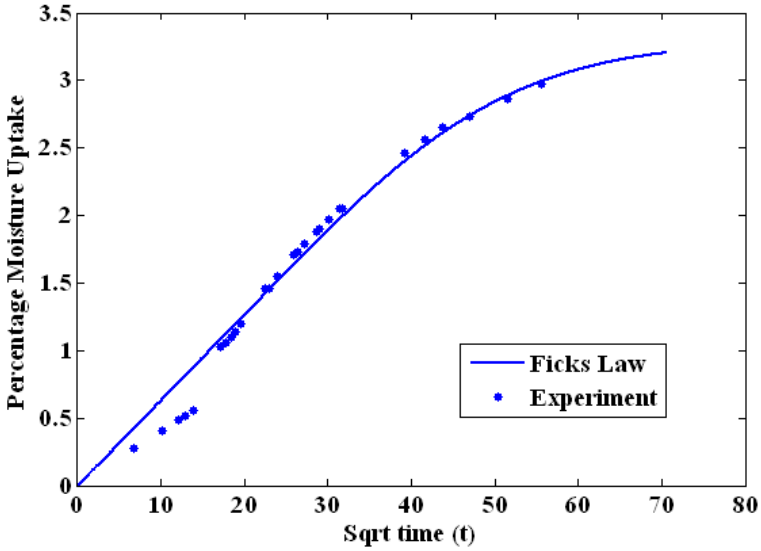

Figure 5.6: Percentage moisture uptake vs Sqrt time (t) for HWS specimens

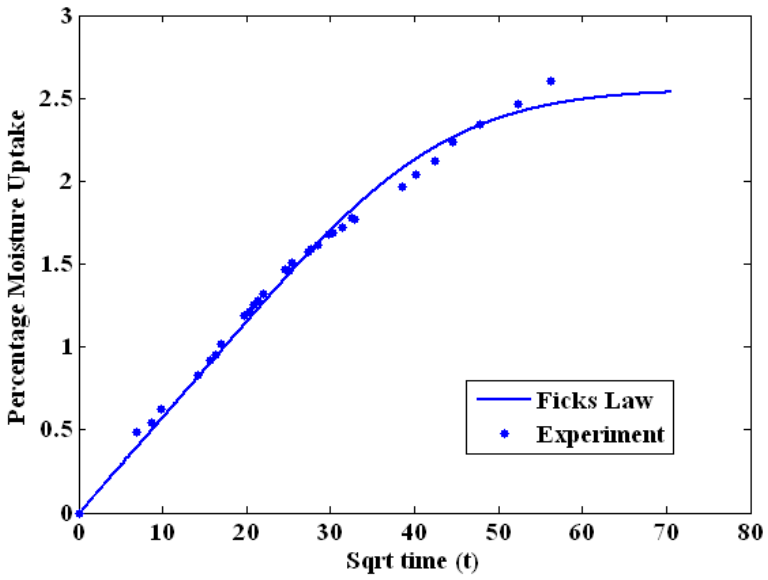

Figure 5.7: Percentage moisture uptake vs Sqrt time (t) for CWS specimens

Figures 5.4 and 5.6 show that all the HWU and HWS specimens absorbed maximum moisture of around 3 %. Figures 5.5 and 5.7 show that all the CWU and CWS specimens absorbed maximum moisture of 2.5 %. Also it is seen that the hot wet specimens absorbed more moisture than the cold wet specimens, which clearly shows the effect of temperature on moisture absorption. Table 5.1 gives the coefficient of diffusion (D) and saturation moisture uptake (M_∞) for each ageing condition.

Table 5.1: Coefficient of Diffusion (D) and Saturation Mass Uptake (M_∞)

Number	Ageing Condition	Exposure Time (days)	Coefficient of Diffusion (D) cm^2/s	Saturation Moisture Uptake (M_∞) gm
1	HWU	178	7.70×10^{-8}	0.0792
2	CWU	131	4.37×10^{-8}	0.0625
3	HWS	129	3.44×10^{-8}	0.0875
4	CWS	132	4.72×10^{-8}	0.0678

5.2. AVERAGE INTERFACIAL BOND STRENGTH ANALYSIS

The Peak Load (N) vs Displacement (mm) plots for the unaged control specimens and accelerated ageing conditions cold dry, cold wet, hot dry, hot wet and stressed; tested at times t_1 and t_2 using the MTS tensile testing machine are shown in figures 5.8 through 5.12.

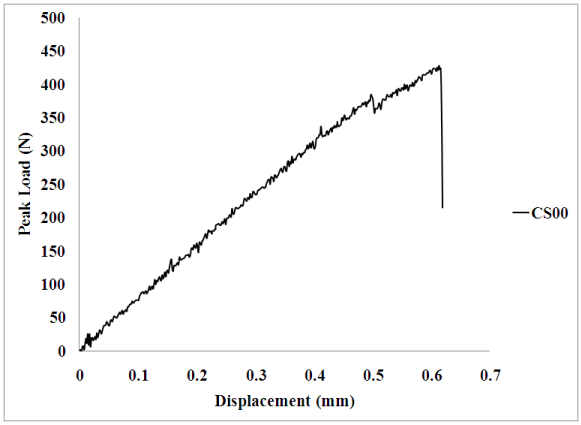

Figure 5.8: Debonding load vs Displacement plots: Unaged control sample at time t_0 (CS00)

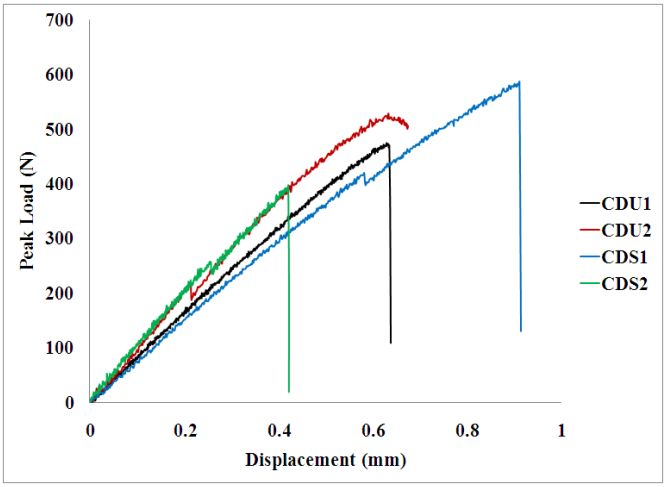

Figure 5.9: Debonding load vs Displacement plots: Cold dry unstressed sample at time t_1 (CDU1), Cold dry unstressed sample at time t_2 (CDU2), Cold dry stressed sample at time t_1 (CDS1) and Cold dry stressed sample at time t_2 (CDS2)

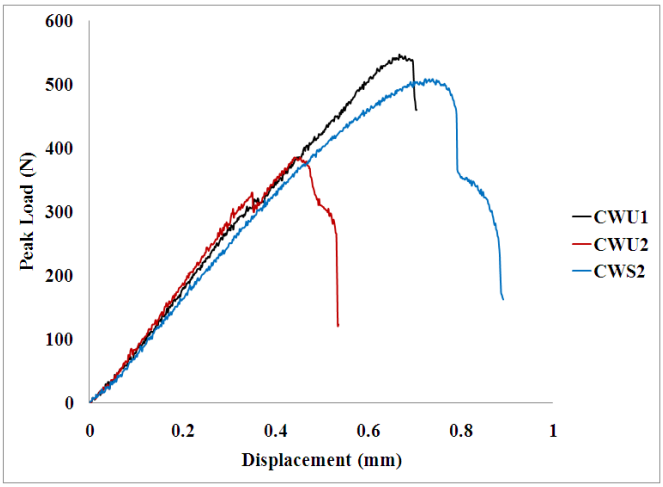

Figure 5.10: Debonding load vs Displacement plots: Cold wet unstressed sample at time t_1 (CWU1), Cold wet unstressed sample at time t_2 (CWU2) and Cold wet stressed sample at time t_2 (CWS2)

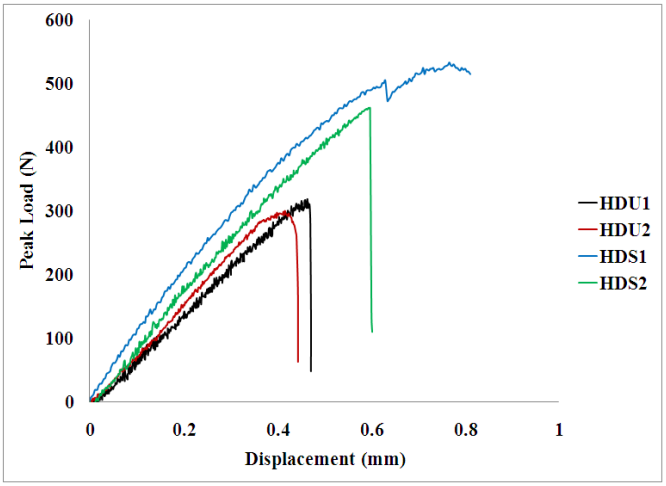

Figure 5.11: Debonding load vs Displacement plots: Hot dry unstressed sample at time t_1 (HDU1), Hot dry unstressed sample at time t_2 (HDU2), Hot dry stressed sample at time t_1 (HDS1) and Hot dry stressed sample at time t_2 (HDS2)

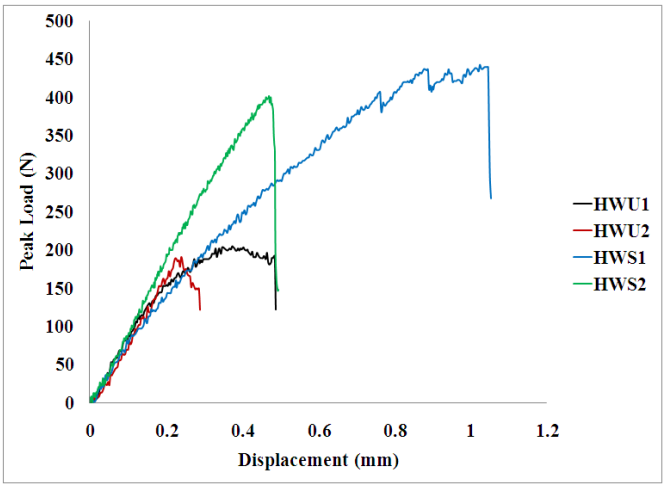

Figure 5.12: Debonding load vs Displacement plots: Hot wet unstressed sample at time t_1 (HWU1), Hot wet unstressed sample at time t_2 (HWU2), Hot wet stressed sample at time t_1 (HWS1) and Hot wet stressed sample at time t_2 (HWS2)

The average IFBS data of all the accelerated aged and unaged control specimens tested at times t_1 and t_2 are provided in figure 5.13. The percentage decreases in average bond strengths compared to unaged control specimens (CS00) are observed from table 5.2.

Figures 5.13 and 5.14 show a variation chart of Average Interfacial Bond Strength for different environmental ageing specimens at time intervals t_0, t_1 and t_2. The IFBS of unaged control specimen (CS00) is observed to be 21.5 MPa. The hot/wet/stressed (70 °C, 3 % M, 2 lb) specimen showed maximum degradation (-31.54 %) in IFBS in comparison to control specimen (CS00). The IFBS of all the specimens continued degradation over extended ageing period (t_1 to t_2) even after reaching saturation state. In some cases increased IFBS is observed in hot and cold dry samples when compared to unaged control sample and this is possibly due to post curing effects of the resin.

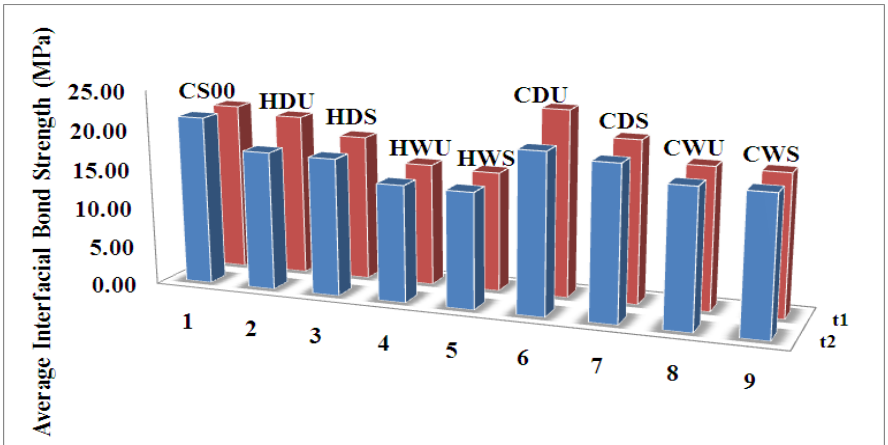

	1	2	3	4	5	6	7	8	9
t2	21.49	17.65	17.49	14.86	14.71	20.33	19.56	17.53	17.49
t1	21.49	20.62	18.55	15.59	15.25	23.74	20.65	18.04	17.94

Figure 5.13: Average interfacial bond strength of specimens

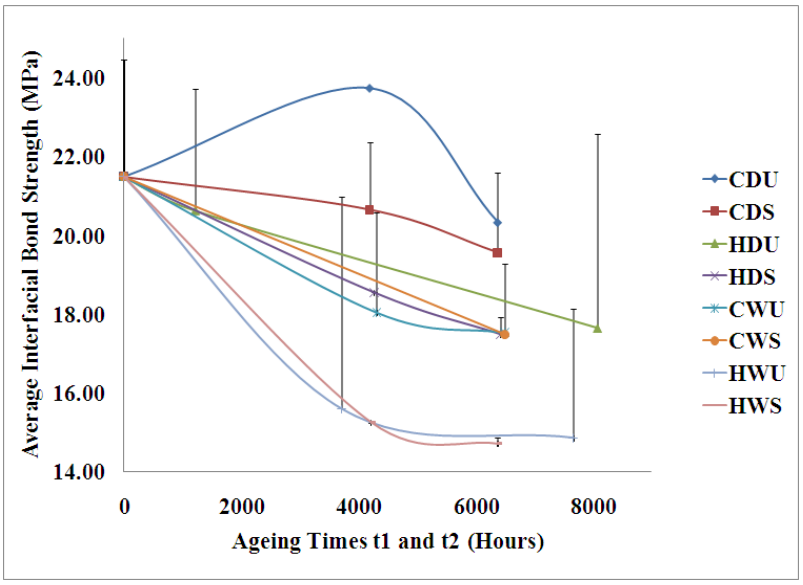

Figure 5.14: Effects of different environmental ageing parameters on interfacial bond strength

Table 5.2: Decrease of Interfacial bond strength of various aged samples compared to (IFBS) of control sample (CS00)/21.5 MPa

Environmental Ageing Condition	Ageing Time t_1 (Hrs)	Average IFBS at t_1	Decrease in Bond Strength at t_1 (%)	Ageing Time t_2 (Hrs)	Average IFBS at t_2	Decrease in Bond Strength at t_2 (%)
HDU	1224	20.62	-4.02	8088	17.65	-17.87
HDS	4272	18.55	-13.67	6432	17.49	-18.62
HWU	3720	15.59	-27.44	7680	14.86	-30.86
HWS	4224	15.25	-29.03	6384	14.71	-31.54
CDU	4200	23.74	10.49	6384	20.33	-5.38
CDS	4200	20.65	-3.89	6384	19.56	-8.98
CWU	4320	18.04	-16.03	6504	17.53	-18.43
CWS	4320	17.94	-16.51	6504	17.49	-18.62

It is observed from Table 5.2 for ageing time t_1 that the decrease in strength of the dry samples HDU1 (-4.02 %), HDS1 (-13.67 %) and CDS1 (-3.89 %) is much less compared to the decrease in strength of the wet samples HWU1 (-27.44 %), HWS1 (-29.03 %), CWU1 (-16.03 %) and CWS1 (-16.51 %). It is evident from this data, that moisture has a highly detrimental effect on the IFBS of the samples. Comparison of HWU1 (-27.44 %), HWS1 (-29.03 %), CWU1 (-16.03 %) and CWS1 (-16.51 %) IFBS data indicates that the applied stress does not have much effect on the degradation of the IFBS strength of the samples within this ageing condition and time regime. Comparison of HDU1 (-4.02 %), HDS1 (-13.67 %), CDU1 (10.49 %) and CDS1 (-3.89 %) shows significant degradation after t_1 ageing time interval due to pre-stressing in both hot and cold specimens. It is to be mentioned that such noticeable degradation was not observed after t_2 ageing time interval.

Comparison of HOT samples like HDU1 (-4.02 %), HDS1 (-13.67 %), HWU1 (-27.44 %) and HWS1 (-29.03 %) with COLD samples like CDU1 (10.49 %), CDS1 (-3.89 %), CWU1 (-16.03 %) and CWS1 (-16.51 %) indicates that the HOT samples have degraded more in strength than COLD samples. HOT samples are aged at higher temperature (70 °C) than COLD samples (50 °C). Therefore, we expect the HOT samples to degrade more in strength than the COLD samples. In CDU1 strength enhancement was observed, which could be explained due to post curing during the ageing (because the post cure temperature of the matrix is 71.1 °C).

Limited strength enhancement at higher temperature, as discussed above, has also been reported by (Detassis et al) and (Reifsnider and Case) for carbon-epoxy composites. Detassis and

his group indicated that the enhancement was the result of superior sizing at higher temperature. But Reifsnider and Case provided an alternative explanation by referring the degradation of interfacial properties due to matrix softening, which in turn reduces stress concentrations, thereby effectively increasing strength. However, in this research, we postulate that the strength enhancement at higher temperature is primarily because of post-curing of the epoxy resin.

It is observed from Table 5.2 for ageing time t_2 that the trend of decrease in strength of the dry samples HDU2 (-17.87 %), HDS2 (-18.62 %), CDU2 (-5.38 %) and CDS2 (-8.98 %) is much less compared to the decrease in strength of the wet samples HWU2 (-30.86 %), HWS2 (-31.54 %), CWU2 (-18.43 %) and CWS2 (-18.62 %) has continued. Again from this data it is evident, that moisture has a highly detrimental effect on the IFBS of the samples. Comparison of HWU2 (-30.86 %), HWS2 (-31.54 %), CWU2 (-18.43 %) and CWS2 (-18.62 %) IFBS data indicates that the applied stress shows little difference on the degradation of IFBS in the samples within this ageing condition and time regime. Comparison of HDU2 (-17.87 %), HDS2 (-18.62 %), CDU2 (-5.38 %) and CDS2 (-8.98 %) also shows little difference on the degradation of IFBS in the samples after t_2 ageing time interval.

Comparison of HOT samples like HDU2 (-17.87 %), HDS2 (-18.62 %), HWU2 (-30.86 %) and HWS2 (-31.54 %) with COLD samples like CDU2 (-5.38 %) CDS2 (-8.98 %), CWU2 (-18.43 %) and CWS2 (-18.62 %) indicates that the HOT samples have degraded more in strength than COLD samples throughout the ageing times t_1 and t_2. HOT samples are aged at higher

temperature (70 °C) than COLD samples (50 °C). Therefore, we expect the HOT samples to degrade more in strength than the COLD samples.

The maximum degradation is seen in hot wet stressed samples HWS2 (-31.54%), which states that the most critical conditions are under high temperatures, exposed to moisture and bearing a stress.

5.2.1. Degradation Mechanism

The results in table 5.2 show significant degradation in IFBS due to moisture, temperature, pre-stressing and synergistic effects of all the ageing parameters. Various mechanisms influenced such degradation in IFBS.

Moisture (de-ionized water) present in the water bath eventually penetrated the interface by diffusion controlled process due to which hydrolysis occurs and the epoxy breaks down. The absorbed water is not liquid, but exists rather in the form of hydrogen-bounded molecules or clusters within the matrix. Hydrolysis is a chemical process in which a molecule is cleaved into two parts by the addition of a molecule of water. One fragment of the parent molecule gains a hydrogen ion (H^+) from the additional water molecule. The other group collects the remaining hydroxyl group (OH^-) as shown in figure 5.15. In the hydrolysis of an amide into a carboxylic acid and an amine or ammonia, the carboxylic acid has a hydroxyl group derived from a water molecule and the amine (or ammonia) gains the hydrogen ion as shown figure 5.16.

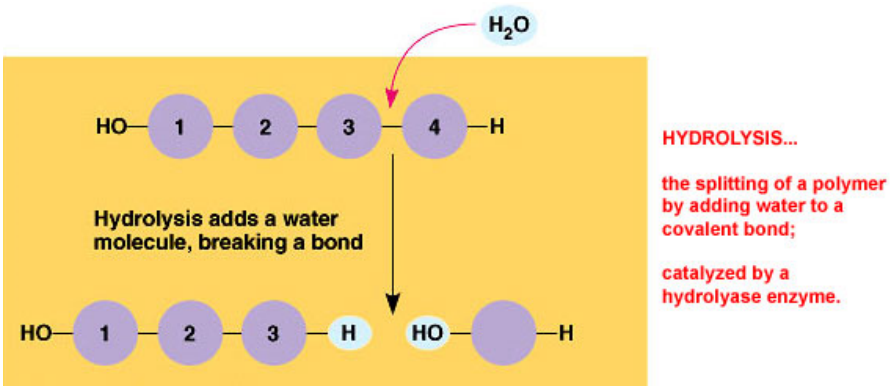

Figure 5.15: Hydrolysis

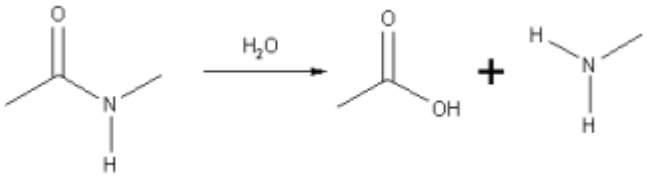

Figure 5.16: Hydrolysis of an Amide

The rate of moisture absorption is seen to have been controlled by the material property called moisture diffusivity. The absorbed water softened the epoxy resin, causing it to swell, and lowered its glass transition temperature (T_g/93.33 for SC-780). In general, moisture causes a lowering of the interfacial bond strength due to softening of bulk matrix and interface materials.

The Carbon fiber pull-out samples were exposed to cold (50 °C) and hot (70 °C) temperatures. Strength and stiffness properties are generally unimpaired at temperatures much lesser than glass transition temperature (T_g). We have seen approximately 17 % degradation in IFBS at elevated temperatures (70 °C). As the temperature is elevated closer to the T_g, the matrix

or interface materials transforms from the glassy state to rubbery state. This eventually softens the matrix material resulting degradation in IFBS.

The results of this study indicate that degradation mechanism of interface becomes more aggressive in the synergistic effects of heat and moisture. We have seen severe damage (31.5 %) due to synergistic effects in hot/wet samples. In such case both moisture and temperature degradation mechanisms acted simultaneously and caused such significant loss of IFBS. Applied heat seems to have caused matrix alterations that allowed the matrix water holding capacity to increase (Hygrothermal deformation).

5.3. MAXIMUM INTERFACIAL BOND STRENGTH ANALYSIS

As mentioned in the previous chapter finite element analysis was done to calculate the maximum interfacial bond strength. Two dimensional (2D) and three dimensional (3D) FEA of fiber tow pull-out test were carried out to determine maximum debond stress at the interface. The 3D FEA was initially carried out without any cohesive elements at the fiber/matrix interface for unaged control samples. In later stages this model was modified to predict degradation due to environmental ageing effects at the interface by incorporating cohesive elements at the interface. The cohesive elements provided the scope to vary the stiffness in the interface for each environmental ageing condition.

5.3.1. Three Dimensional Finite Element Model

A 3D FEA of the carbon fiber tow pull-out test has been done using ABAQUS code. The FEA model was developed with and without cohesive layer element at the interface. Since the fiber tow is assumed to be approximately rectangular in cross section, the distribution of debond stress is observed to be different in width and thickness sections. Figures 5.17 and 5.18 show highlighted thinner and wider sections of the carbon fiber tow.

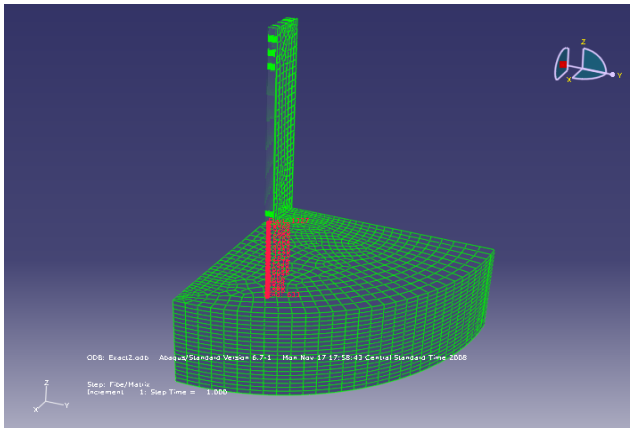

Figure 5.17: Thinner section in the 3D FEA model

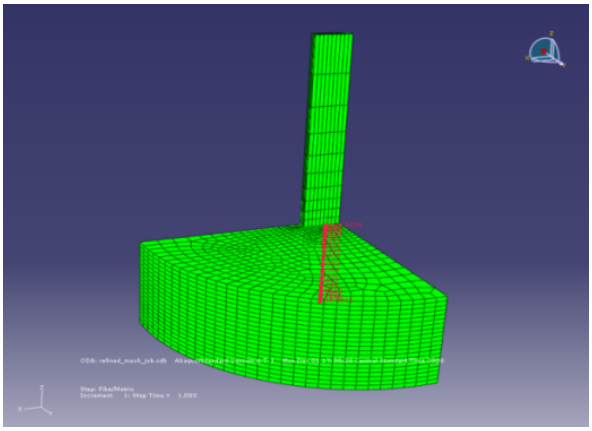

Figure 5.18: Wider section in the 3D FEA model

5.3.2. Three Dimensional Finite Element Model without Cohesive Elements at the Interface

Firstly, a 3D FEA model without any cohesive elements at the fiber/matrix interface was developed as shown in figures 5.17 and 5.18. The applied stress was similar to experimental data obtained for the unaged control sample as mentioned in the previous chapter.

Figure 5.19 shows applied stress vs displacement plots from the experiment and finite element simulations which show good agreement. It is to be noted that the applied load in FEA was one fourth of the total failure load shown in the experiment due to quarter symmetric model.

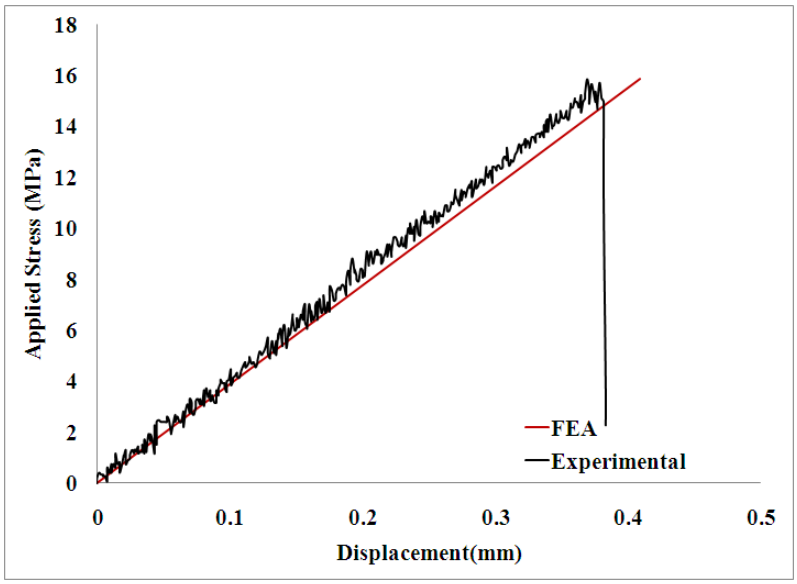

Figure 5.19: Comparison of Applied stress vs Displacement plot from FEA and Experimental testing

5.3.3. Effects of various Parameters of the fiber and matrix on IFBS

In this section the effects of embedded fiber length, matrix modulus, fiber modulus, volume fraction of the fiber on IFBS have been investigated individually for both the thinner and the wider sections of the fiber tow as shown in figures 5.20 through 5.27.

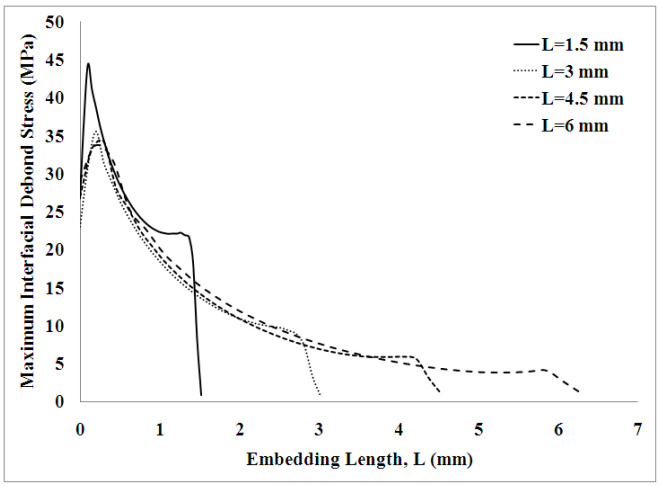

Figure 5.20: Maximum interfacial shear stress variations with different embedding lengths in the thinner section

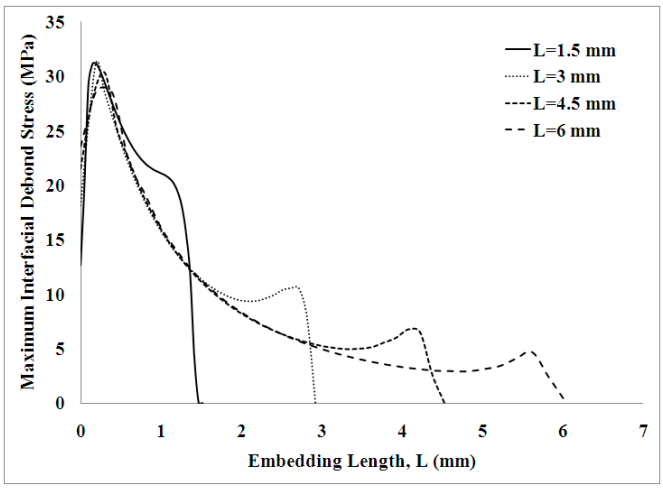

Figure 5.21: Maximum interfacial shear stress variations with different embedding lengths in the wider section

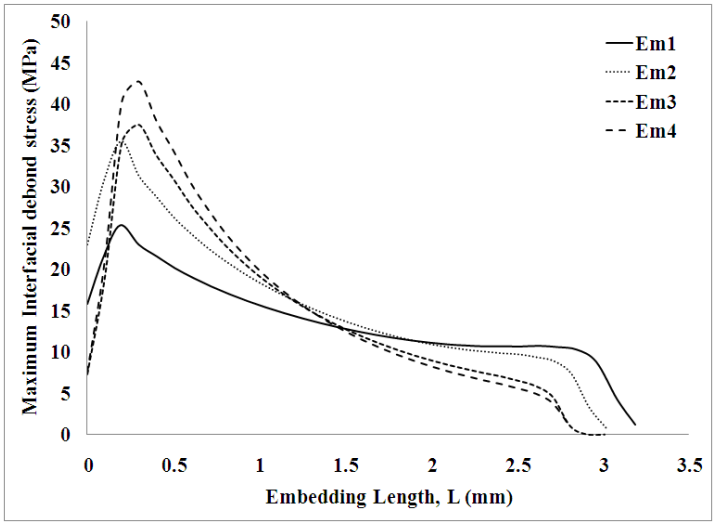

Figure 5.22: Maximum Interfacial Shear Stress variations with different Matrix Modulus values in the thinner section

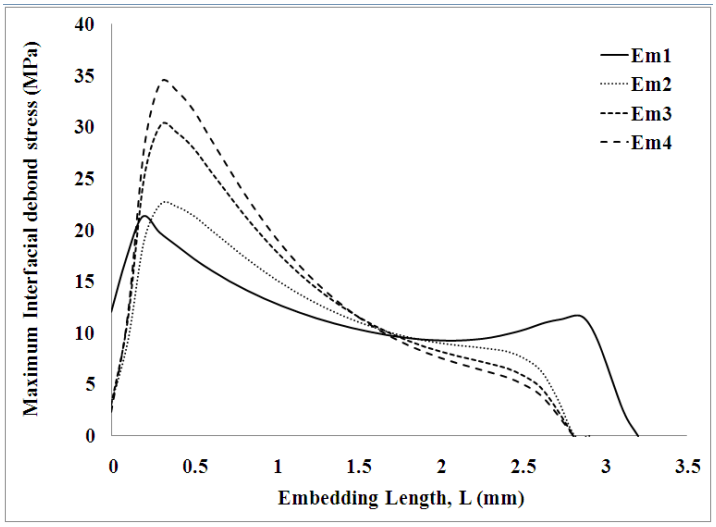

Figure 5.23: Maximum Interfacial Shear Stress variations with different Matrix Modulus values in the wider section

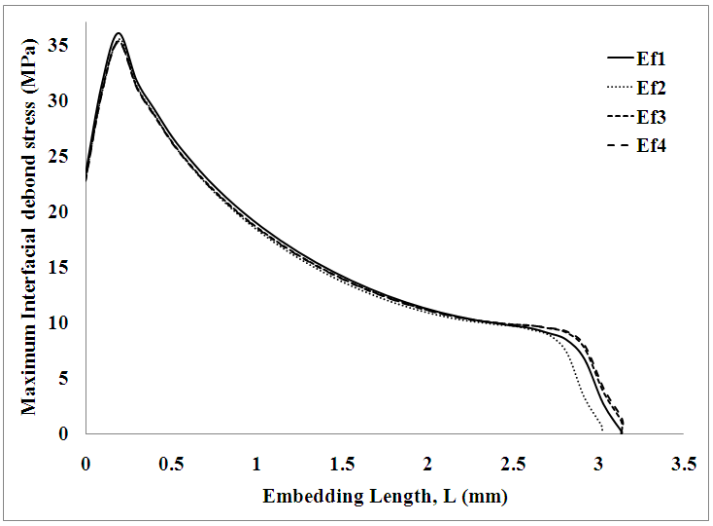

Figure 5.24: Maximum Interfacial Shear Stress variations with different Fiber Modulus values in the thinner section

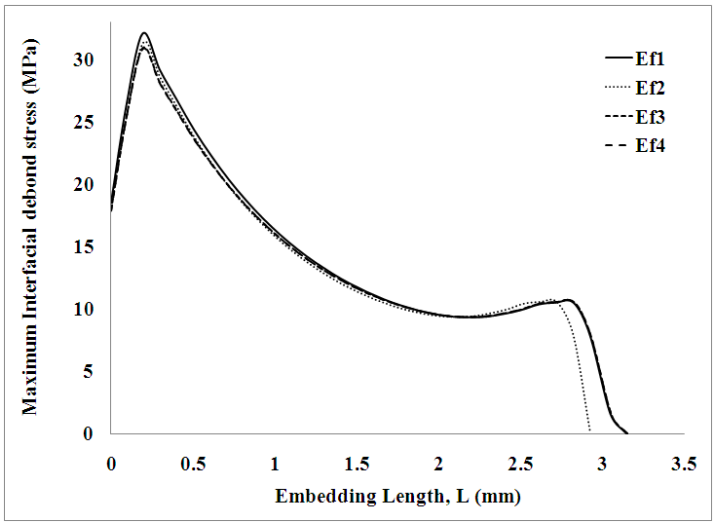

Figure 5.25: Maximum Interfacial Shear Stress variations with different Fiber Modulus values in the wider section

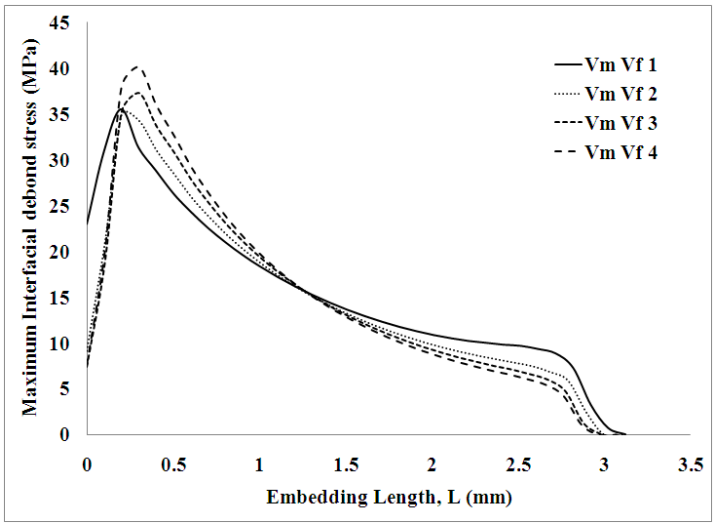

Figure 5.26: Maximum Interfacial Shear Stress variations with different Fiber and Matrix Volume fractions in the thinner section

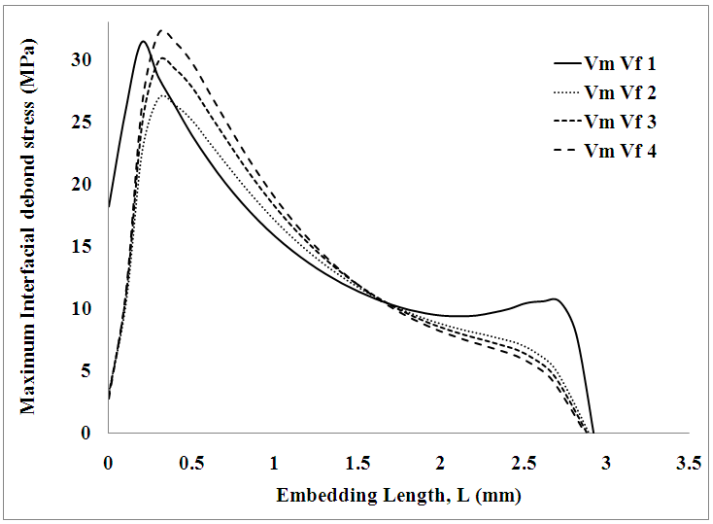

Figure 5.27: Maximum Interfacial Shear Stress variations with different Fiber and Matrix Volume fractions in the wider section

Tables 5.3 and 5.4 show the variation of Maximum IFBS by varying the different parameters that have been mentioned earlier. Alternating columns in the tables give IFBS values pertaining to each other the parameter.

Table 5.3: Variation of IFBS with different parameters in the thinner section

Length (mm)	**τ_{max} (MPa)**	**E_m (MPa)**	**τ_{max} (MPa)**	**E_f (MPa)**	**τ_{max} (MPa)**	**V_m**	**V_f**	**τ_{max} (MPa)**
1.5	44.39	$0.5E_m$	25.30	$0.5E_f$	31.38	0.2	0.8	35.51
3	35.51	E_m	35.51	E_f	35.51	0.3	0.7	34.92
4.5	34.16	$2E_m$	37.51	$2E_f$	35.27	0.4	0.6	37.28
6	33.71	$3E_m$	42.68	$3E_f$	35.22	0.5	0.5	40.17

Figure 5.20 shows plots of interfacial shear stress distribution in thinner section for different embedded lengths (1.5 mm, 3 mm, 4.5 mm & 6 mm) of the carbon fiber tow in epoxy resin. A maximum IFBS of 44.39 MPa was observed in case of 1.5 mm fiber embedded length. The samples with fiber embedded lengths 3mm, 4.5 mm and 6 mm show IFBS 35.51 MPa, 34.16 MPa and 33.71 MPa, respectively. It shows that the max. IFBS is less sensitive as the embedded length increases from 3 mm to 6 mm. Typically, max. IFBS are seen near the fiber tow insertion point.

Figure 5.22 shows the effects of matrix stiffness on the IFBS of fiber tow in the thinner section. The maximum IFBS is seen to increase almost 20 % as the matrix modulus increases from E_m to $3E_m$. A significant reduction (30%) in max. IFBS is observed as the matrix modulus decreases from E_m to 0.5 E_m.

Figure 5.24 shows that variation of fiber stiffness has no effects on the IFBS of carbon fiber tow embedded in epoxy matrix. This is reasonable since IFBS is a matrix dominant property.

Figure 5.26 shows the effects of matrix volume fractions (20% to 50%) on the IFBS in the thinner section. The simulation results show slight increase (13%) in max. IFBS as the V_m increases from 20 % to 50%. Similar pattern of the interfacial stress along the fiber length was also observed in paper by Kim et al.

Table 5.4: Variation of IFBS with different parameters in the wider section

Length (mm)	**τ_{max} (MPa)**	**E_m (MPa)**	**τ_{max} (MPa)**	**E_f (MPa)**	**τ_{max} (MPa)**	**V_m**	**V_f**	**τ_{max} (MPa)**
1.5	31.15	$0.5E_m$	21.27	$0.5E_f$	32.06	0.2	0.8	31.35
3	31.35	E_m	22.49	E_f	31.35	0.3	0.7	26.94
4.5	30.38	$2E_m$	30.19	$2E_f$	30.95	0.4	0.6	29.86
6	28.67	$3E_m$	34.30	$3E_f$	30.82	0.5	0.5	32.09

The debonding is seen to initiate at the insertion point of the fiber tow and gradually proceeding along the length of the fiber tow at the interface region. Table 5.4 shows maximum IFBS simulated data recorded from the wider section of the fiber tow as a function of embedded length, matrix modulus, fiber modulus and volume fraction of the matrix. Comparing IFBS in the thinner and the wider section, it is seen that the stress is more dominant on the thinner section than on the wider section.

Figure 5.21 shows IFBS distribution as a function of embedded length along the wider section of the fiber tow. The simulated maximum IFBS data show little variation with increased embedded length ranging from 1.5 mm to 6 mm. It is to be noted that the maximum IFBS in the wider section is seen to be comparatively less than the same in the thinner section. The IFBS distribution along the embedded length shows gradual decrease from the maximum IFBS value along the length of the fiber tow until it reaches near the other end of the fiber. The magnitude at the valley of IFBS distribution plot is seen to decrease with increased embedded length. In case of 6 mm embedded fiber length IFBS magnitude at fiber end is very close to zero.

Figures 5.23 and 5.25 show IFBS distribution as a function of matrix modulus and fiber modulus in the wider section of the tow. The FEA simulation represents increased IFBS with increased matrix modulus, but no significant variation in IFBS is observed with the variation of fiber modulus. In all the cases the trend of IFBS plots are almost simillar in both wider and thinner sections of the fiber tow.

Figure 5.27 shows IFBS distribution plots as a function of volume fraction of the matrix in the wider section of the tow. The maximum IFBS is observed to increase slightly with increased volume fraction of the matrix in the range 0.3 to 0.5.

5.3.4. Three Dimensional Finite Element Model with Cohesive Elements at the Interface

After observing reasonable agreement from the FEA model without cohesive elements the FEA model with the cohesive elements was developed. This model allowed to simulate the

separation or debond at the fiber matrix interface after the fiber pull out test as shown in figure 5.28. It also allowed to incorporate the degradation effects due to the environment at the interface.

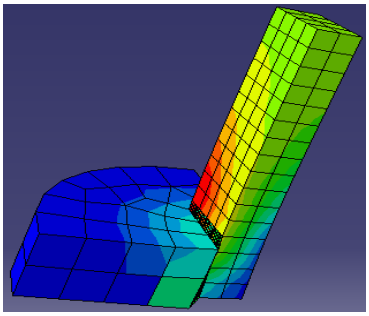

Figure 5.28: Separation at the interface on fiber pull-out test

The material properties and loading conditions were varied for different ageing conditions based on experimental results. Table 5.5 shows the material properties and loads used for the unaged control sample (CS00) and the different aged samples after t_1 period.

Table 5.5: Loads and Material Properties *for CS00 and t_1 ageing conditions*

Ageing Condition	**Peak Load (N)**	**E**	**G1**	**G2**	**N_3**	**N_1**	**N_2**
CS00	504.42	69	34	29	80	70	50
HDU1	390.98	160	98	85	80	40	45
HDS1	586.92	120	30	30	60	38	30
CDU1	440.66	110	40	40	70	60	35
CDS1	554.35	120	26	22	65	50	40
HWU1	306.98	110	40	30	40	25	20
HWS1	448.99	80	18	18	55	24	20
CWU1	572.01	130	30	30	60	34	30

The FEA model can be calibrated if the Experimental Applied Stress vs Displacement plots match the same plots from the FEA model. Figures 5.29 through 5.36 shows comparison of Applied Stress vs Displacement plots from experiments and finite element simulations for unaged control sample (CS00) and different t_1 ageing conditions.

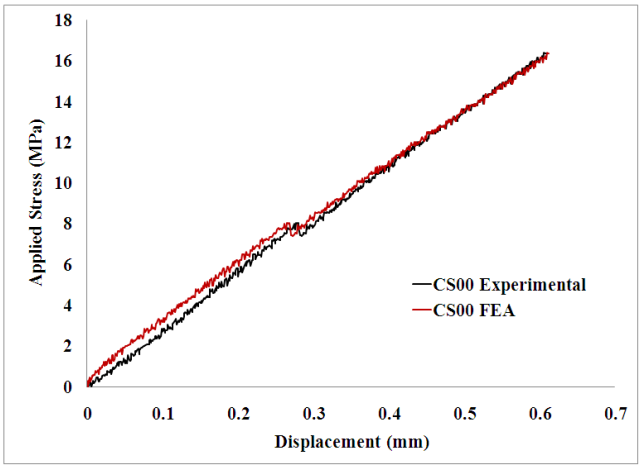

Figure 5.29: Comparison of Applied Stress vs Displacement plot from FEA and Experimental testing for Unaged Control sample (CS00)

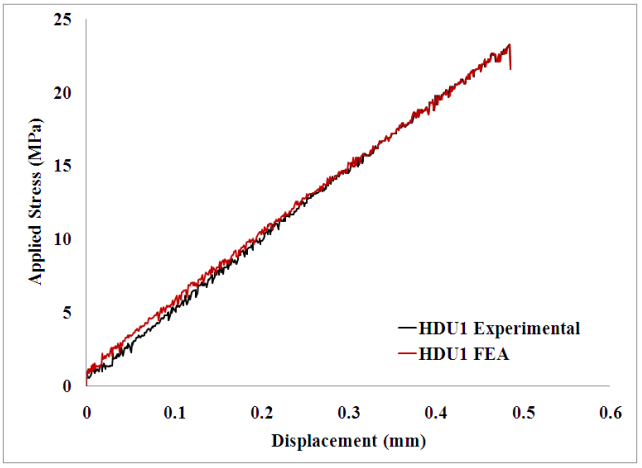

Figure 5.30: Comparison of Applied Stress vs Displacement plot from FEA and Experimental testing for Hot Dry Unstressed sample at time t_1 (HDU1)

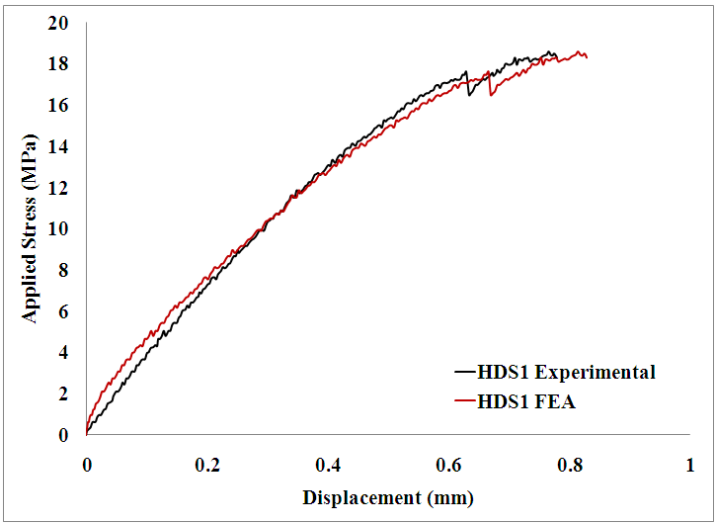

Figure 5.31: Comparison of Applied Stress vs Displacement plot from FEA and Experimental testing for Hot Dry Stressed sample at time t_1 (HDS1)

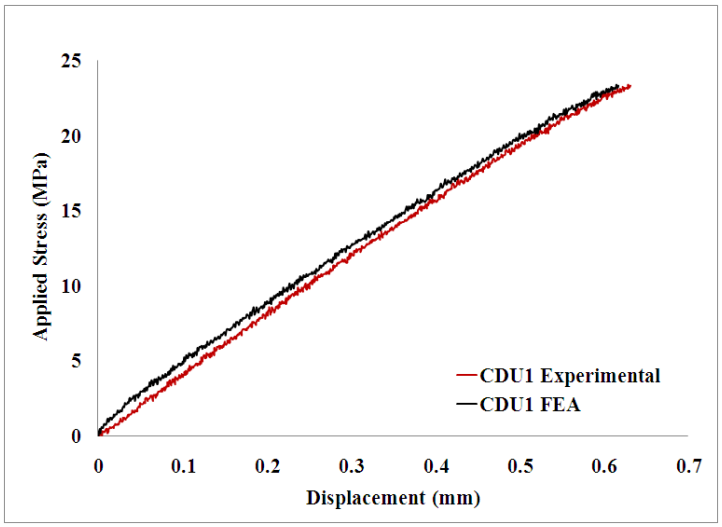

Figure 5.32: Comparison of Applied Stress vs Displacement plot from FEA and Experimental testing for Cold Dry Unstressed sample at time t_1 (CDU1)

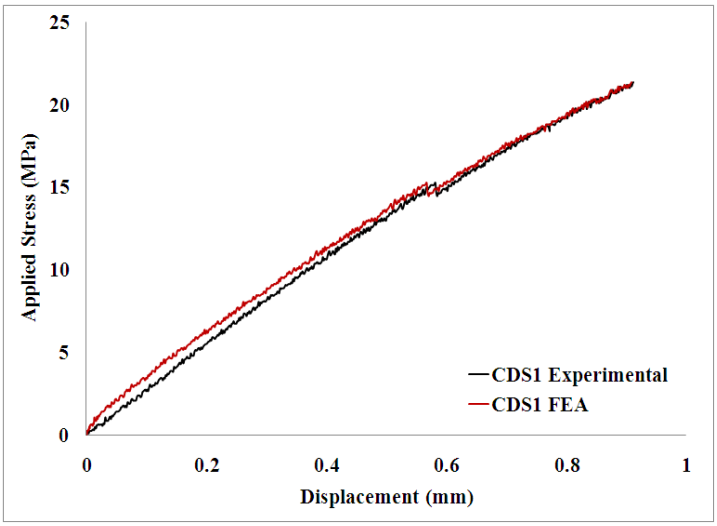

Figure 5.33: Comparison of Applied Stress vs Displacement plot from FEA and Experimental testing for Cold Dry Stressed sample at time t_1 (CDS1)

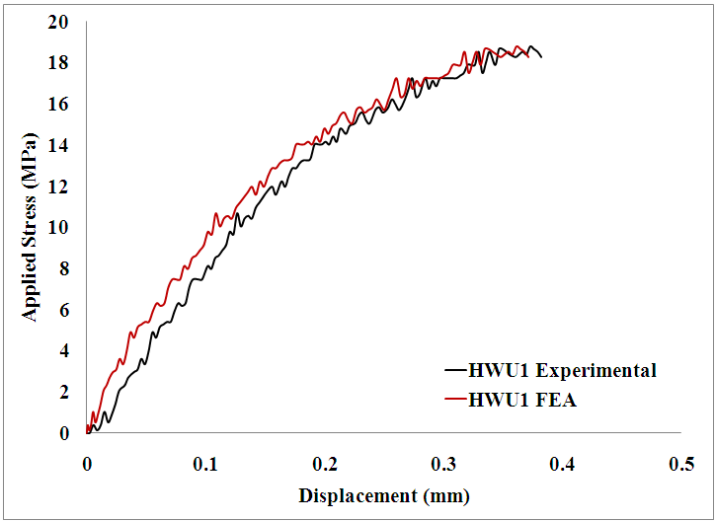

Figure 5.34: Comparison of Applied Stress vs Displacement plot from FEA and Experimental testing for Hot Wet Unstressed sample at time t_1 (HWU1)

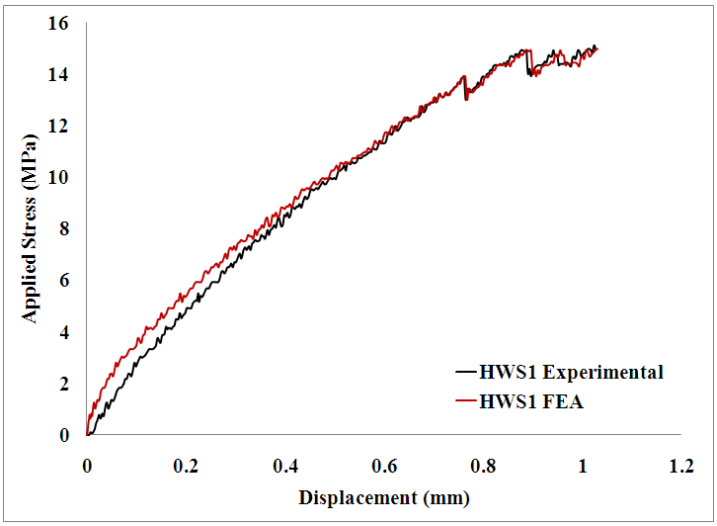

Figure 5.35: Comparison of Applied Stress vs Displacement plot from FEA and Experimental testing for Hot Wet Stressed sample at time t_1 (HWS1)

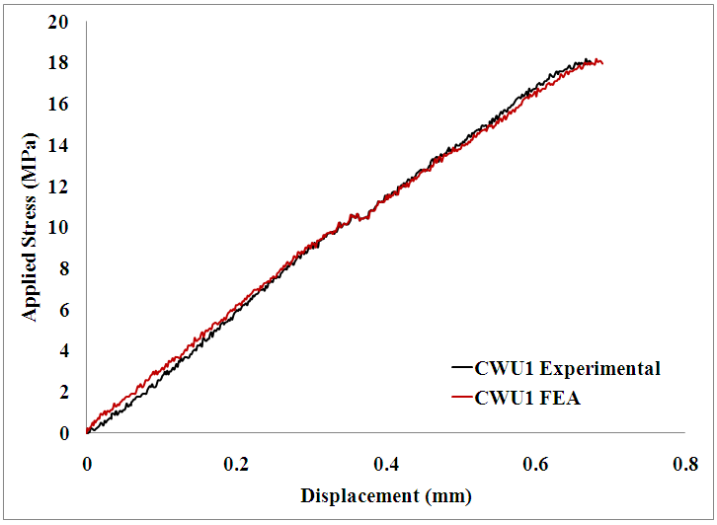

Figure 5.36: Comparison of Applied Stress vs Displacement plot from FEA and Experimental testing for Cold Wet Unstressed sample at time t_1 (CWU1)

Table 5.6 shows the applied stress and material properties used to perform FEA simulations under t_2 ageing conditions. Figures 5.37 through 5.44 shows comparison of Applied

Stress vs Displacement plots from experiments and finite element simulations under t_2 ageing conditions.

Table 5.6: Loads and Material Properties for t_2 ageing conditions

Ageing Condition	Peak Load (N)	E	G1	G2	N_3	N_1	N_2
HDU2	300	90	38.5	20	50	35	20
HDS2	461.81	75	37.5	22	60	34	30
CDU2	547.69	100	35.5	22	60	39	30
CDS2	398.45	98	72	58	50	40	30
HWU2	190	51	64	44	45	24	20
HWS2	401.11	65	41	36	50	23	20
CWU2	384.22	80	65	57	46	29	29
CWS2	508.07	60	23	20	52	28	25

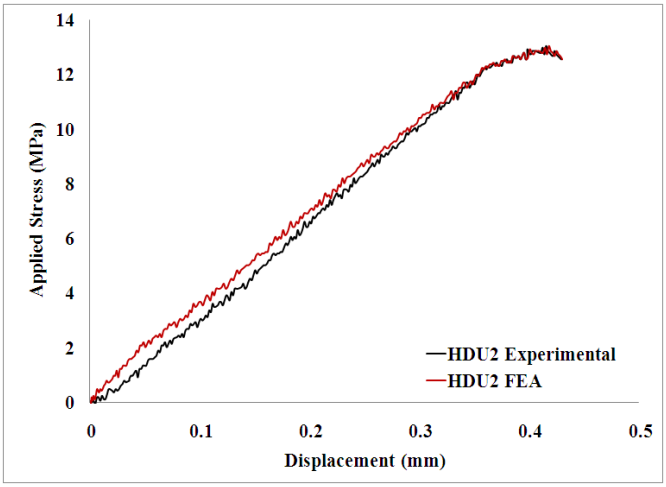

Figure 5.37: Comparison of Applied Stress vs Displacement plot from FEA and Experimental testing for Hot Dry Unstressed sample at time t_2 (HDU2)

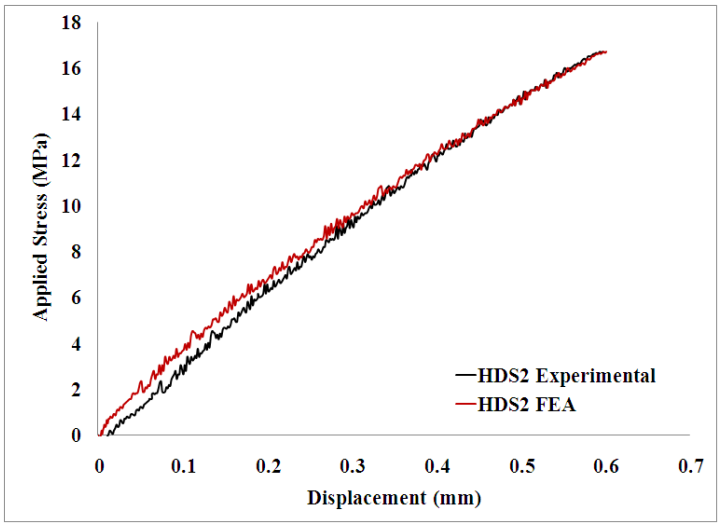

Figure 5.38: Comparison of Applied Stress vs Displacement plot from FEA and Experimental testing for Hot Dry Stressed sample at time t_2 (HDS2)

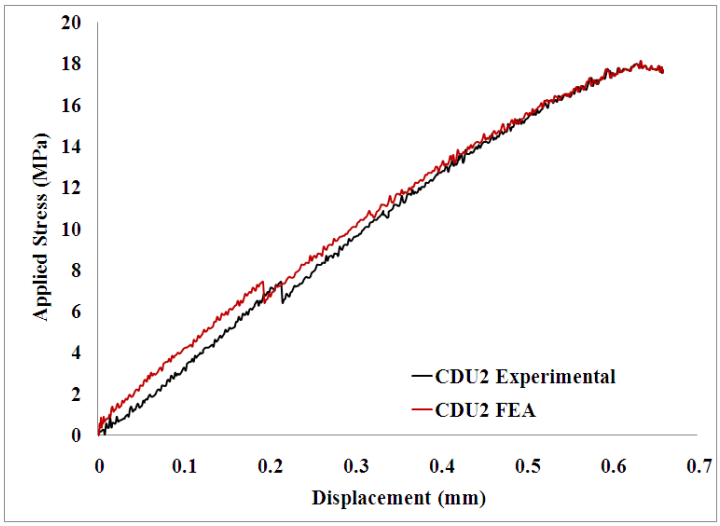

Figure 5.39: Comparison of Applied Stress vs Displacement plot from FEA and Experimental testing for Cold Dry Unstressed sample at time t_2 (CDU2)

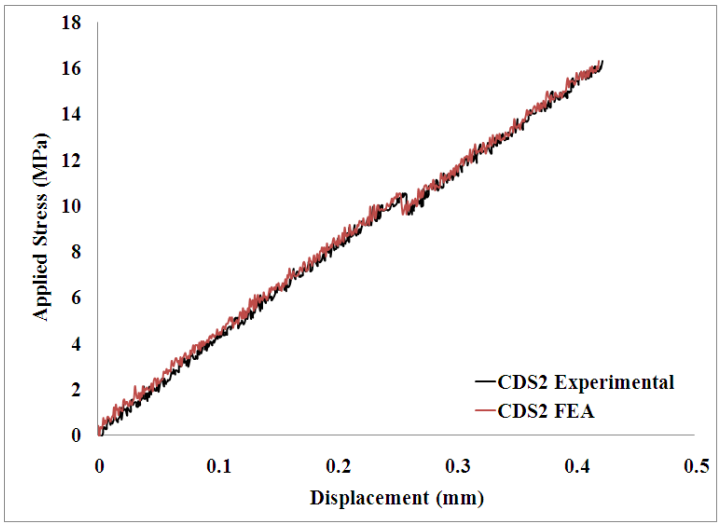

Figure 5.40: Comparison of Applied Stress vs Displacement plot from FEA and Experimental testing for Cold Dry Stressed sample at time t_2 (CDS2)

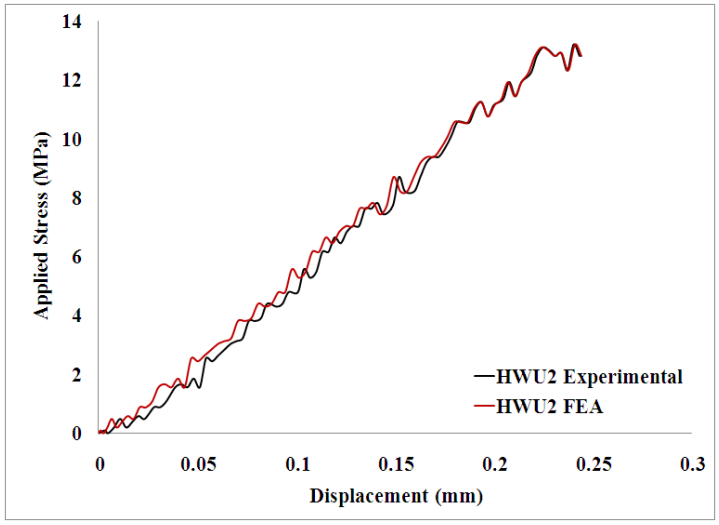

Figure 5.41: Comparison of Applied Stress vs Displacement plot from FEA and Experimental testing for Hot Wet Unstressed sample at time t_2 (HWU2)

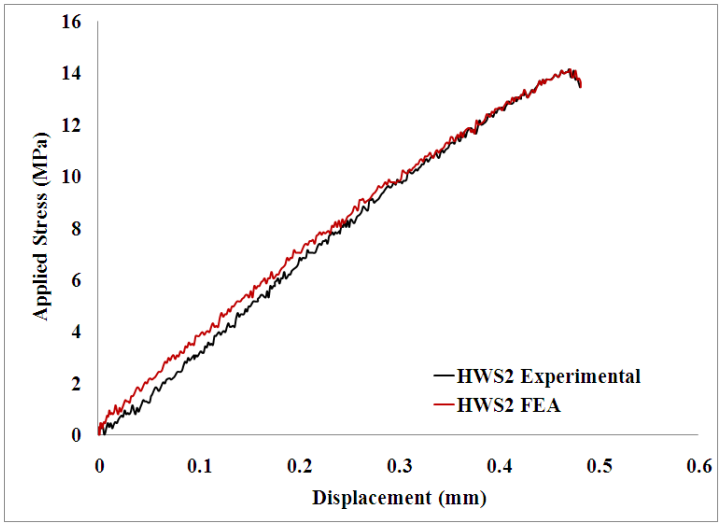

Figure 5.42: Comparison of Applied Stress vs Displacement plot from FEA and Experimental testing for Hot Wet Stressed sample at time t_2 (HWS2)

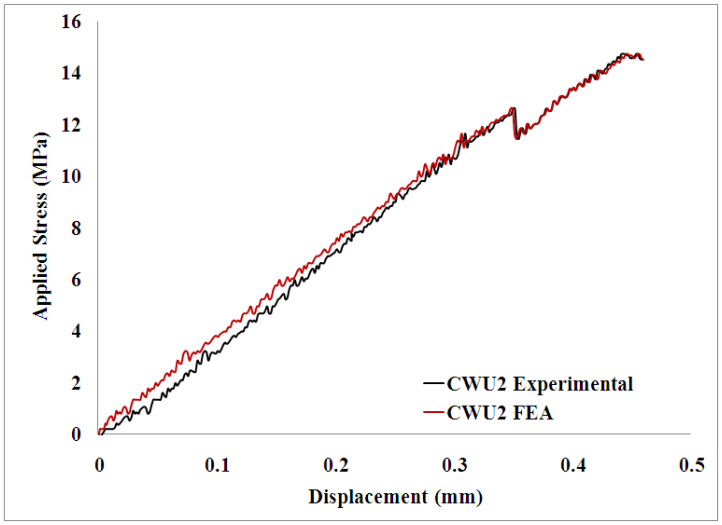

Figure 5.43: Comparison of Applied Stress vs Displacement plot from FEA and Experimental testing for Cold Wet Unstressed sample at time t_2 (CWU2)

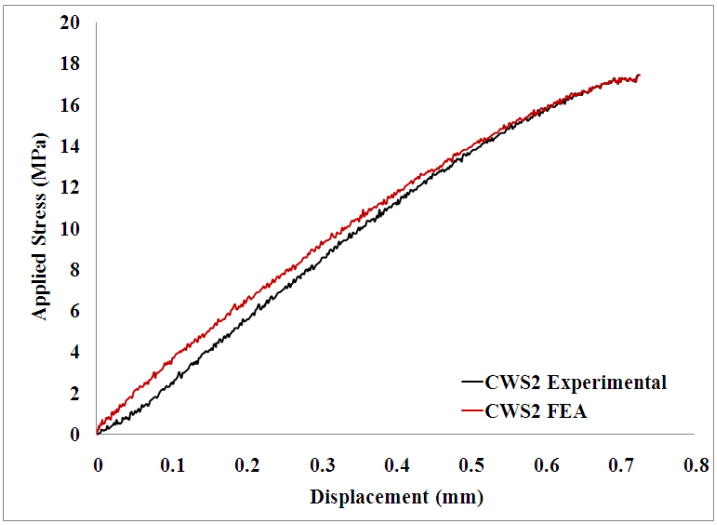

Figure 5.44: Comparison of Applied Stress vs Displacement plot from FEA and Experimental testing for Cold Wet Stressed sample at time t_2 (CWS2)

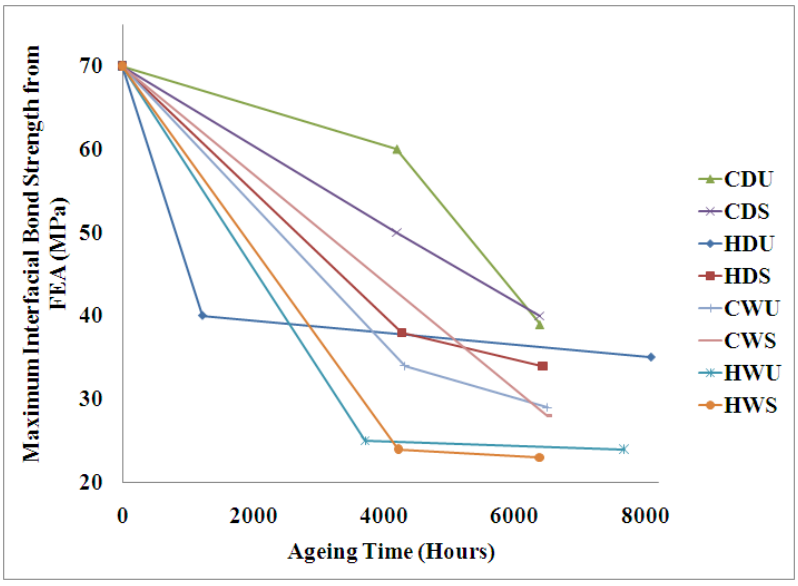

Figure 5.45: Maximum IFBS (MPa) vs Ageing Time (t1 and t2 in hours) plot

Figures 5.29-5.44 show good agreement between FEA simulations of applied stress vs displacement plots of aged specimens with the experimental testing results. And figure 5.45 shows the maximum IFBS (MPa) (N_1 in the previous tables 5.6 and 5.7) vs ageing time (t_1 and t_2 in hours) plot. The trend of degradation in IFBS with time is similar to the trend seen in experimental data. The most degrading condition from FEA is hot/wet/stressed condition.

5.4. FIBER PULL-OUT TEST - FAILURE MODES

Fiber pull-out test of the tow clearly showed debonding of the fiber tow from the matrix as shown in figure 5.46. This shows reasonable justification that pull-out test of single fiber tow may be used to determine approximately the interfacial bond strength of fiber reinforced polymer (FRP) composites. It is to be noted that most of the FRP composites use woven fabric architecture which consists of fiber tow configuration as an entity at larger scale. Each single fiber tow eventually consists of 6000 single filaments. The complexity of single fiber pull-out test particularly under synergistic environmental effects and the fracture mode observed in this study show a promise to determine interfacial bond strength of FRP composites from single fiber tow pull-out test.

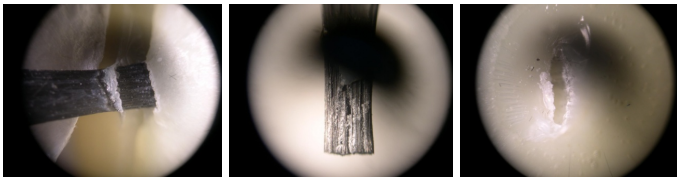

(a) *(b)* *(c)*

Figure 5.46: (a) Picture of the partially pulled out fiber from the resin, (b) Completely pulled out fiber after testing and (c) The fiber embedding portion in the resin after pull out

It is worth mentioning that in some specimens cracking in bulk matrix is observed followed by interfacial debonding. In such cases a chunk of matrix is seen to be attached like a neck with the fiber tow near the insertion region. Some of the specimens also show meniscus at the insertion point as shown in figure 5.47. This meniscus was formed during the processing stage of a single fiber tow specimens. In most cases specimens with meniscus initially show fracture in the matrix and then the crack propagates through the interface region as shown in figure 5.46 (a). The meniscus is seen to be attached with some specimens after interfacial bond fracture. We have discarded the test data if interfacial bond failure is not observed in the fracture mode.

A method was devised to reduce the meniscus at the entry point with the help of two metal plates. These were held in position by the aid of two spring clamps. The whole set up was kept inverted during curing in order to get a flat surface at the fiber entry region as shown in figure 5.48. This was done to investigate whether there is a significant effect of meniscus on the bond strength of carbon fiber tow embedded in epoxy resin.

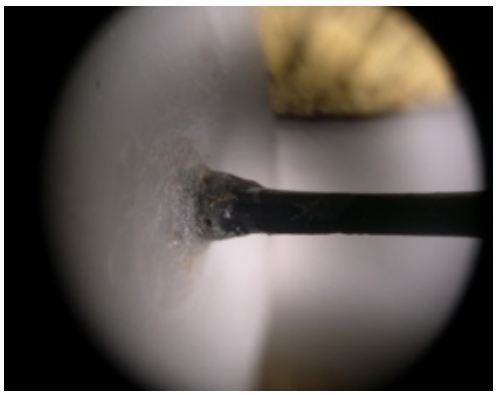

Figure 5.47: Resin meniscus at the fiber insertion point

Figure 5.48: Meniscus removing device

5.5. COMPARISON OF FIBER PULL-OUT SPECIMENS WITH MENISCUS AND WITHOUT A MENISCUS

The above mentioned specimen manufacturing technique was used to have fiber tow pull out specimens without a meniscus. This was done in order to investigate whether there is a significant effect of meniscus on the bond strength of carbon fiber tow embedded in epoxy resin.

5.5.1. Specimen test matrix

The specimens with and without meniscus were subjected to five different environmental ageing conditions. Each of those is tabulated in Table 5.7, H hot (70°C), C cold (50°C), W wet (immersed in de-ionized water), D dry (dry) and U unstressed

Table 5.7: Sample designation as per ageing condition

Environmental Exposure Condition	Number of Specimens
Unaged (Control)	4 CS00
Cold/dry/unstressed	4 CDU
Cold/wet/unstressed	4 CWU
Hot/dry/unstressed	4 HDU
Hot/wet/unstressed	4 HWU

The average IFBS data of all the accelerated aged and unaged control specimens are provided in table 5.8. The percentage decreases in average bond strengths compared to unaged control specimens (CS00) are observed from table 5.8.

Table 5.8: Decrease of Interfacial bond strength of various aged samples compared to (IFBS) of control sample (CS00)/24.10 MPa

Environmental Ageing Condition	**Average IFBS (MPa)**	**Decrease in Bond Strength at t_1 (%)**
HDU1	21.42	-2.69
HWU1	16.61	-7.49
CDU1	23.01	-1.10
CWU1	22.91	-1.19

It is observed from Table 5.8 that the trend of decrease in strength of the dry samples HDU1 (-2.69 %) and CDU1 (-1.10 %) is much less compared to the decrease in strength of the wet samples HWU1 (-7.49 %) and CWU1 (-1.19 %). Again from this data it is evident that

moisture has a highly detrimental effect on the IFBS of the samples as seen in samples with meniscus.

Comparison of HOT samples like HDU1 (-2.69 %) and HWU2 (-7.49 %) with COLD samples like CDU2 (-1.10 %) and CWU2 (-1.19 %) indicates that the HOT samples have degraded more in strength than COLD samples. HOT samples are aged at higher temperature (70 °C) than COLD samples (50 °C). Therefore, we expect the HOT samples to degrade more in strength than the COLD samples similar to the samples with meniscus.

Also, the maximum degradation is seen in hot wet unstressed samples HWU1 (-7.49%), which states that the most devastating conditions are under high temperatures, exposed to moisture, similar to the trend seen in samples with meniscus.

Figure 5.49 shows a variation chart of average interfacial bond strength for different environmental ageing specimens and for specimens with meniscus and without meniscus. The IFBS of unaged control specimen (CS00 at time t_1) is observed to be 21.49 MPa for sample with meniscus and the IFBS of unaged control specimen (CS00) is observed to be 24.10 MPa for sample without meniscus. Similar to the trend observed in samples with meniscus the hot/wet/unstressed (70 °C, 4.4 % M) specimen without meniscus showed maximum degradation (-7.49 %) in IFBS in comparison to control specimen (CS00).

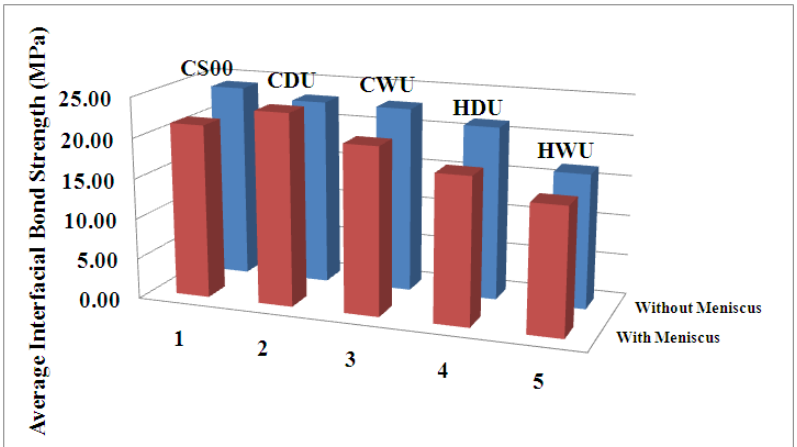

	1	2	3	4	5
With Meniscus	21.49	23.74	20.62	18.04	15.59
Without Meniscus	24.10	23.01	22.91	21.42	16.61

Figure 5.49: Effects of different environmental ageing parameters in interfacial bond strength of carbon fiber tow embedded in epoxy resin and Comparison of IFBS in samples with meniscus and without meniscus

It is seen in figure 5.49 that specimens without meniscus show comparatively higher strength (9 %) than specimens with meniscus. Such increase in IFBS for the specimens without meniscus is not very significant. It is to be noted that the specimen with meniscus often show partial interfacial debonding having a small chunk of matrix material attached to the fiber tow. But in calculating the average IFBS, we have considered the total interfacial area which is truly not the case when partial pull-out takes place. As a result the IFBS data for the specimen with meniscus show lesser value in figure 5.49. True estimation of pull-out area should minimize such discrepancy. On this basis it is concluded that the effects of meniscus on IFBS of single fiber pull out test is not significant.

CONCLUSIONS

The fiber tow pull-out (FTP) tests have been successfully carried out to study synergistic environmental effects such as moisture, temperature and pre-stressed conditions in FRP composites. It is seen that the manufactured samples desorbs almost 0.23% moisture contents after dessication at 70°C for a period of four weeks. The data for moisture absorption under eight environmental aged conditions have been generated. Maximum moisture absorption of 3.25 % is observed in case of hot/wet/unstressed (most degrading condition) samples after 180 days of exposure period. The average interfacial debond strength of all the samples have been determined through FTP tests. The results show that the maximum degradation (32% / 266 days) in bond strength occurred under hot/wet/stressed condition. Typically, samples exposed to hot conditions show more degradation than the ones exposed to cold conditions. The reason for such higher degradation in bond strength at hot condition (70 °C) is due to the softening of interfacial materials. In case of dry conditions the pre-stress effect is noticeable but a very little difference is observed in stressed specimen compared to unstressed specimen in the wet conditions. In such case moisture effects dominate pre-stressing on IFBS. Also, the results show that the dry conditions have lesser degrading effect than the wet conditions. The evidence of fiber tow pull-out was clearly observed under the pull-out tests. In some cases cracking was observed in the bulk matrix followed by interfacial debonding of the fiber tow. A chunk of matrix is seen to be attached with the fiber tow after complete pull-out of the fiber tow.

The 3D finite element model was developed for the single fiber tow pull-out specimens with and without cohesive element. The applied stress (σ) vs displacement (δ) plots were

simulated under different synergistic environmental aged conditions. The FEA σ- δ predicted results were compared with experimental data. An excellent agreement was observed between FEA and experimental results. All the degraded orthotropic material constants under different environmental aged conditions are predicted which will be used in developing a long term durability analysis code for FRP composites. The FEA model with cohesive element successfully showed pull-out of the single fiber tow from the matrix materials. The pull-out is seen to be initiated at the insertion region of the fiber tow in the resin. Similar fracture mode was also observed in the experiment.

REFERENCES

Abbasi and P.J. Hogg, “Temperature and environmental effects on glass fibre rebar: modulus, strength and interfacial bond strength with concrete”, Composites Part B 36 (2005), pp. 394–404.

Andreevskaya G. D. & Gorbatkina Y. A., Ind. Eng. Chem., Prod. Res. Develop. 11, 1 (1972) 24-26.

Chua P. S. & Piggott M. R., Composites Science & Technology 22 (1985) 33-42; 107-119; 185-196.

Detassis, M., A. Pegoretti and C. Migliaresi. "Effect of temperature and strain rate on interfacial shear stress transfer in carbon/epoxy model composites", Composites Science and Technology (1995): 39-46.

D.L. Caldwell, D.A. Babbington and C.F. Johnson, “Interfacial bond strength determination in manufactured composites”. In: F.R. Jones, Editor, Interfacial Phenomena in Composite Materials, Butterworth (1989), pp. 42–52.

Eagles D. B., Blumentritt B. F. & Cooper S. L., J. of Applied Polymer Science 20 (1976) 435-448.

Emandipour H., Chiang P. & Koenig J. L., Res Mechanica 5 (1982) 165-176.

Faber, K.T., Advani, S.H., Lee, J.K. and Jinn, J.T., 1986, “Frictional Stress Evaluation along the Fiber-Matrix Interface in Ceramic Matrix Composites”, J. of American Ceramics Society, 699, pp. C-208–C-209.

Favre J.-P. & Perrin J., J. of Materials Science 7 (1972) 1113-1118.

Favre J.-P. & Mérienne M.-C., Int. J. Adhesion & Adhesives, October 1981, 311-316.

Favre J. P, “Review of test methods and testing for assessment of fibre-matrix adhesion”. In: F.R. Jones, Editor, Proc. Int. Conf. on Interfacial Phenomena in Composite Materials '89, Butterworths, London (1989), pp. 7–12.

Goruganthu S., Elwell J., Ramasetty A., Nair A.R., Roy S., Haque A., Dutta P.K. and Kumar A., (2008) “Characterization and Modeling of the Effect of Environmental Degradation on Interlaminar Shear Strength of Carbon/Epoxy Composites”. Polymers and Polymer Composites, Vol. 16, No. 3, p.165-179.

Grande, D.H., Mandell, J.F. and Hong, K.C.C., 1988, “Fiber-Matrix Bond Strength Studies of Glass, Ceramic and Metal Matrix Composites”, J. of Matls. Science, 23, pp. 311–328.

Haque A and S. Jeelani, “Environmental Effects on the Compressive Properties: Thermosetting vs. Thermoplastic Composites”, Journal of Reinforced Plastics and Composites, Vol. 11/February, pp.146-157, (1992).

Haque A, S. Mahmood, L. Walker and S. Jeelani,” Moisture and Temperature Induced Degradation in Tensile Properties of Kevlar- Graphite/Epoxy Hybrid Composites”, Journal of Reinforced Plastics and Composites, Vol.10-March, pp. 132-145, (1991).

Haque A, Copeland C.W., Zadoo D.P and Jeelani S.,” Hygrothermal Influence on the Flexural Properties of Kevlar-Graphite/Epoxy Hybrid Composites”, Journal of Reinforced plastics and Composites, 9 (1990), 602-613.

Kazuto Tanaka, Kohji Minoshima, Witold Grela and Kenjiro Komai. “Characterization of the aramid/epoxy interfacial properties by means of pull-out test and influence of water absorption”, Composites Science and Technology,Volume 62, Issue 16, December 2002, Pages 2169-2177.

Kim, J. K., Zhou, L. M. Bryan, S. J. and Mai, Y. W. (1994 b). Effect of fiber volume fraction on Interfacial debonding and fiber pull out. Composites 25, 470-475.

Mai Y. W. & Castino F., J. of Materials Science Letters 4 (1985) 505-508.

Nardin M. & Ward I. M., Materials Science & Technology 3 (1987) 814-826.

Nishiyabu, K., Yokoyama, A., and Zako, M., 1997, “Assessment of Interfacial Stress Transfer Mechanisms in Single Fiber Pull-out test by Using Numerical Analysis”, Advances in ComputationalEngineering Science, ed. S.N. Atluri and G. Yagawa, Tech Science Press, pp. 1299–1304.

Penn L. S. & Lee S. M., Fibre Science & Technology 17 (1982) 91-97.

Penn L. S., Bystry F. A. & Marchionni H. J., Polymer Composites 4, 1 (1983) 26-31.

Penn L. S. & Liao T. K., Composites Technology Rev. 6, 3 (1984) 133-136.

Penn L. S., Bystry F., Karp W. & Lee S., in “Molecular Characterization of Composite Interfaces”, Ishida H. & Kumar G., ed., 1985, op. cit., 93-109.

Peters, P. M. W., “A New Method to determine the fiber-Matrix Bond Strength” Proceedings of Interfacial Phenomena in Composite Materials ’89, F. R. Jones, Ed., Buttersworths, London, 1989, pp. 59-62.

Piggott M. R., Sanadi A., Chua P. S. & Andison D., in “Composite Interfaces”, Ishida H. & Koenig J. L., ed., 1986, op. cit., 109-121.

Piggott M. R. & Andison D., J. of reinforced Plastics & Composites 6 (1987) 290-302.

Pitkethly M. J and J.B. Doble. “Characterizing the fibre/matrix interface of carbon fibre-reinforced composites using a single fibre pull-out test”, Composites, Volume 21, Issue 5, September 1990, Pages 389-395.

Pochiraju, K., 1993, “Mechanics of the Single Fiber Pullout Problem with Several Interface Conditions”, Ph.D. Dissertation, Drexel University.

Reifsnider, Kenneth L. and Scott Case. “Mechanics of temperature-driven long-term environmental degradation of polymer-based composite systems”. American Society of Mechanical Engineers, Materials Division (Publication) MD (1995): 225-230.

Shao-Yun Fu, Chee-Yoon Yue, Xiao Hua, Yiu-Wing Mai. “Analyses of the micromechanics of stress transfer in single- and multi-fiber pull-out tests”, Composites Science and Technology 60, Issue 4, 2000, Pages 569-579.

Shiriajeva G. V. & Andreevskaya G. D., Soviet Plastics, 4 (1962) 40-42.

Subramanian R. V. & Shu K. H., in “Molecular Characterization of Composite Interfaces”, Ishida H. & Kumar G., ed., 1985, op. cit., 205-236.

Sun, W. and Lin, F., “Computer Modeling and FEA Simulation for Composite Single Fiber Pull-out”, Journal of Thermoplastic Composite Materials, Vol. 14, 2001, pp. 1-17.

Ward I. M. & Ladizesky N. H., Pure & Appl. Chem. 57, 11 (1985) 1641-1649.

Wells J. K. & Beaumont P. W. R., J. of Materials Science 20 (1985) 1275-1284.

W. Janssens, L. Doxsee Jr., I. Verpoest and P. de Meester In: F.R. Jones, Editor, Interfacia phenomena in Composite Materials’89, Butterworths, London (1989), pp. 147–154.

APPENDIX A

MATLAB CODE TO EVALUATE COEFFICIENT OF DIFFUSION (D) AND SATURATION MOISTURE UPTAKE (M_∞) FOR A GIVEN SET OF EXPERIMENTAL DATA

```
%%%%%%%%%%%%%%%%%%%%%%%%%%%%%%%%%%%%%%%%%%%%%%
```

The inputs to this MATLAB code are thickness of diffusion (l), input file for experimental data (hwu-ficks-data.txt), number of data points (k). Coefficient of Diffusion (D) and Saturation moisture uptake (M_∞) are outputted by this code.

```
%%%%%%%%%%%%%%%%%%%%%%%%%%%%%%%%%%%%%%%%%%%%%%
clc
clear all
l=2.54*0.20 ;             %  thickness of diffusion in  cm
f=50;                     % number of terms in fourier series
syms D  n;                %  D is diffusivity cm^2/sec
digits(5);
% input experimental data for moisture uptake in gm and time in hours
%------------------------------------------------------------------------------------------------------
expdata=load('hwu-ficks-data.txt')   % input file for experimental data
t=3600*expdata(:,1);              % t is in secs
Mk=expdata(:,2);                  % Mk is moisture uptake (gm) at given time
k = 40;                           % number of data points
```

```
%-------------------------------------------------------------------------------------------------
%initialisation
%-------------------------------------------------------------------------------------------------
sigmakMk=0;
sigmakAMk=0;
sigmakA=0;
sigmakAsquare=0;
sigmakB=0;
sigmakBMk=0;
sigmakBA=0;
%-------------------------------------------------------------------------------------------------
% terms required in Minf evaluation
 %-------------------------------------------------------------------------------------------------
for i=1:1:k
    A(i)=vpa(symsum((exp((-D).*(2*n+1).^2.*pi.^2.*t(i)./l.^2)/(2*n+1).^2),n,0,f));
    sigmakMk=vpa(sigmakMk+Mk(i));
    AMk(i)=vpa(A(i).*Mk(i));
    sigmakAMk=sigmakAMk+AMk(i);
    sigmakA=vpa(sigmakA+A(i));
    Asquare(i)=vpa(A(i).*A(i));
```

```
    sigmakAsquare=sigmakAsquare+Asquare(i);
   %-------------------------------------------------------------------------------------------------
   % terms required in f(D) evaluation
   %-------------------------------------------------------------------------------------------------
    B(i)=vpa(symsum((exp((-D).*(2*n+1).^2.*pi.^2.*t(i)./l.^2).*t(i)),n,0,f));
    sigmakB=vpa(sigmakB+B(i));
    BMk(i)=vpa(B(i).*Mk(i));
    sigmakBMk=sigmakBMk+BMk(i);
    BA(i)=vpa(B(i).*A(i));
    sigmakBA=sigmakBA+BA(i);
   %-----------------------------------------------------------------------
 end
Minf=vpa((sigmakMk-((8/pi^2).*sigmakAMk))./(k-
((16/pi.^2).*sigmakA)+((64./pi.^4).*sigmakAsquare)));
x=vpa((Minf.^2.*sigmakB)-(Minf.*sigmakBMk)-(0.811.*sigmakBA.*Minf.^2));
%using Minf from above equation to get another
% equation only as a function of D
% write the f(D) into an output file
fid=fopen('output_hwu.txt','w');
fprintf(fid,'%s',char(x));
```

fclose(fid)

% %%%

After running the code, open the output_hwu.txt file and copy the matter in it. Type

f = inline (‘and paste the matter from output_hwu.txt here’) in the MATLAB command window and hit enter. Now,

D = fzero (f,10^-7)

Minfinity = subs(Minf,D)

%%

APPENDIX B

MATLAB CODE TO PLOT EXPERIMENTAL MOISTURE UPTAKE VS SQRT (T) DATA WITH FICKS LAW

% %%

The inputs to this code are Coefficient of Diffusion (D), Saturation Moisture Uptake (M_∞), input experimental data file (hws-ficks-data.txt), number of datapoints (datapoints), thickness of diffusion (l), and initial weight of sample (m0) during experiment. The code generates a plot of experimental moisture uptake vs sqrt (time) and ficks law as output.

%%%

```
clc
clear all
digits(4);
Minf=0.8468;      % Saturation moisture uptake (gm)
D=1.01*10^-7 ;    % Coefficient of Diffusion (cm^2/s)
l=2.54*0.20;      % thickness of diffusion (cm)
syms n;
datapoints=25;    % number of data points
k=1800;           % time
M0 = 22.4416;     % initial weight of sample (m0) during experiment (gm)
Mk(1)=0;
```

```
t(1)=0;
for i=2:1:k
    t(i)=3600*i;
    A(i)=vpa(symsum((exp((-D).*(2*n+1).^2.*3.14.^2.*t(i)/l.^2)/((2*n+1).^2)),n,0,25));
    Mk(i)=vpa(Minf.*(1-0.811.*A(i))) ;
    Mk1(i)=(Mk(i).*100)./M0;
    Mk2=double(Mk1);
end
expdata=load('hws-ficks-data.txt')   % input data file from experiment
t1=3600*expdata(:,1);
Mt=expdata(:,2);
for i=1:1:datapoints
Mt1(i)=(Mt(i)*100)./M0
end
plot(sqrt(t./3600),Mk2)
hold on
plot(sqrt(t1./3600),Mt1,'*')
xlabel('sqrt(t)')
ylabel('percentage moisture uptake')
```